Quantum chaos on the separatrix of the periodically perturbed Harper model

Alice C. Quillen[1] and Abobakar Sediq Miakhel[1]

[1]*Department of Physics and Astronomy, University of Rochester, Rochester, NY, 14627, USA*

(*Electronic mail: aquillen@ur.rochester.edu,amiakhel@u.rochester.edu)

(Dated: 20 December 2024)

We explore the relation between a classical periodic Hamiltonian system and an associated discrete quantum system on a torus in phase space. The model is a sinusoidally perturbed Harper model and is similar to the sinusoidally perturbed pendulum. Separatrices connecting hyperbolic fixed points in the unperturbed classical system become chaotic under sinusoidal perturbation. We numerically compute eigenstates of the Floquet propagator for the associated quantum system. For each Floquet eigenstate we compute a Husimi distribution in phase space and an energy and energy dispersion from the expectation value of the unperturbed Hamiltonian operator. The Husimi distribution of each Floquet eigenstate resembles a classical orbit with a similar energy and similar energy dispersion. Chaotic orbits in the classical system are related to Floquet eigenstates that appear ergodic. For a hybrid regular and chaotic system, we use the energy dispersion to separate the Floquet eigenstates into ergodic and integrable subspaces. The distribution of quasi-energies in the ergodic subspace resembles that of a random matrix model. The width of a chaotic region in the classical system is estimated by integrating the perturbation along a separatrix orbit. We derive a related expression for the associated quantum system from the averaged perturbation in the interaction representation evaluated at states with energy close to the separatrix.

We explore the relation between closely related periodically varying classical and quantum systems containing both regular and chaotic behavior. Our systems are confined in phase space, allowing a finite dimension for the associated quantum system, facilitating computation of the Floquet propagator, and giving potential applications in quantum computing. Husimi distributions showing the structure of eigenstates in phase space of the quantum system are remarkably similar to classical orbits. We find that the dispersion of the unperturbed energy function or operator locates ergodicity in both classical and quantum settings. We estimate the width of the ergodic region in the quantum system, deriving a quantum counterpart to a classical estimate.

I. INTRODUCTION

Classical Hamiltonian dynamical systems can exhibit remarkable complexity with both regular and chaotic dynamics (e.g., Chirikov [15]). A quantum mechanical system, that is derived from or related to a classical one, can exhibit phenomena that is related to the classical dynamics. Eigenfunctions, called quantum scars, can be found in the vicinity of the periodic orbits of the classical system[4,24] and along a separatrix orbit[46]. It has been conjectured[8] that the eigenvalue statistics of a quantum system derived from a classical chaotic one can be described by random matrix theory, whereas the eigenvalue statistics of a quantum system derived from a classical integrable system follows Poisson statistics[5]. At large kick strengths, the quantum kicked rotor, related to the classical kicked rotor and the standard map, can be mapped to an Anderson-type model with a quasi-disordered potential[19] and exhibits a quasi-energy spectrum resembling the Wigner-Dyson form that is characteristic of the Gaussian orthogonal ensemble (GOE) random matrix model[16,26].

Time-periodic driving is a potentially powerful tool for controlling the material properties and dynamics of quantum systems[43] and for carrying out quantum computations[1,18]. In this paper we are interested in the relationship between periodic chaotic classical systems and their quantum discrete counterparts. We choose to study evolution in finite dimensional quantum systems to facilitate numerical computations and because these systems would be relevant for control of quantum systems used for quantum computing.

The Melnikov method establishes the existence of chaotic behavior in a classical Hamiltonian dynamical system under periodic perturbation[36]. The integral of a sinusoidal perturbation near the separatrix orbit of the unperturbed system can be used to generate a map, known as a separatrix map, giving an estimate of the width of a chaotic region[15,48,53,54,57,64]. This approach was used to derive a condition for chaotic behavior known as the Chirikov resonance-overlap criterion[15]. Quantized versions of separatrix maps can exhibit dynamical localization[10,25]. Yampolsky et al.[63] in their study of a perturbed quantum system of hard core particles in a box, recently have shown that the presence of quantum chaos can be estimated from a classical resonance-overlap criterion. We similarly explore the possibility that classical techniques for estimating the location of chaotic regions in phase have quantum counterparts, but in periodically perturbed systems which are also known as Floquet systems (e.g., Neufeld et al.[37]).

We desire a finite dimensional Hamiltonian model that that we can visualize and quantize, and that exhibits adjustable regular and chaotic behavior. We choose a variant of the periodically perturbed pendulum model that was used by Chirikov[15] to derive the criterion, known as the resonance overlap criterion, for the onset of chaotic motion in deterministic classical Hamiltonian systems. That particular system is

a pendulum, with Hamiltonian $H_0(\phi,p) = a\frac{p^2}{2} - \varepsilon\cos\phi$, that is perturbed with a periodic function, giving the time dependent and periodic Hamiltonian (equation 4.50 by Chirikov[15]);

$$H(\phi,p,t)_{\text{PertPend}} = a\frac{p^2}{2} - \varepsilon\cos\phi - \mu(\cos(\phi + vt) + \cos(\phi - vt)). \quad (1)$$

A weak perturbation, with $\mu < \varepsilon$, drives instability at the separatrix of the unperturbed system. The system has three resonances, centered at $p = 0, \pm v/a$ with strengths set by ε and μ, respectively. The frequency of libration about the fixed point at $p = 0, \phi = 0$ in the unperturbed system (with $\mu = \mu' = 0$) is

$$\omega_0 = \sqrt{\varepsilon a}. \quad (2)$$

The coordinate angle $\phi \in [0, 2\pi)$ is periodic, but the momentum $p \in \mathbb{R}$.

The perturbed pendulum model of equation 1 is similar to the kicked rotor;

$$H(\phi,p,t)_{\text{KickedRotor}} = \frac{p^2}{2} - \varepsilon\cos\phi\, D_T(t) \quad (3)$$

where $D_T(t)$ is the Dirac comb, consisting of an infinite sum of delta functions, each separated by period T. The kicked rotor, when mapped at the period T and with momentum p restricted to a periodic interval, generates the well known *standard map*, also introduced by Chirikov[15].

The kicked rotor can be quantized by replacing ϕ, p with linear operators that operate on vectors in a Hilbert space,[13,44]. The quantum model can be restricted to a discrete (or finite dimensional) rather than continuous Hilbert space by choosing eigenstate solutions that are periodic in p[16].

The Harper model, with Hamiltonian $H(\phi,p) = \cos p + \cos\phi$, is a doubly periodic model used to describe the motion of electrons in a 2-dimensional lattice in the presence of a magnetic field[22]. While the Harper model is regular (integrable because it is 2-dimensional and the Hamiltonian is conserved), a generalization of this model, called the kicked Harper model, can exhibit chaotic behavior[29];

$$H(\phi,p,t)_{\text{KickedHarper}} = A\cos p + B\cos\phi\, D_T(t), \quad (4)$$

where $D_T(t)$ is again the Dirac comb and A, B are real coefficients. The kicked Harper model exhibits both regular and chaotic orbits, similar to the kicked rotor, but its phase space is a torus $\phi, p \in [0, 2\pi)$ (e.g., Lévi and Georgeot[31]). Usually the phase space for the Harper model is a coordinate and a momentum, both confined on a periodic lattice, but here we have written the coordinate as an angle, so the associated momentum is an action variable and the model looks similar to the kicked rotor. For small p, the kinetic term $1 - \cos p \sim \frac{p^2}{2}$ and in the same form as the kinetic energy of a harmonic oscillator or pendulum. As is true for the quantized kicked rotor, in the kicked Harper model, when the perturbation is high enough that the associated classical system is chaotic, the statistics of the quasi-energies of the Floquet propagator are similar to that of a random matrix model[59].

An advantage of the Harper model is that its Hamiltonian is periodic in both momentum and coordinate, so phase space is compact and equivalent to a torus. In our study we modify the Harper model to resemble the perturbed pendulum of equation 1. This gives a classical Hamiltonian model on the torus with an adjustable chaotic separatrix width that we can compare with discrete quantized versions.

A. Classical Sinusoidally Perturbed Harper Model

We take a base Harper model (equation 3) but add to it perturbations of the perturbed pendulum model (equation 1). We restore units so that we can later compare classical and quantum system with evolution that depends upon the reduced Planck's constant, $\hbar$. The perturbed Harper model,

$$K(\phi,L,t)_{\text{PH}} = a_K\left(1 - \cos\left(\frac{L}{L_0}\right)\right) - \varepsilon_K\cos(\phi) - \mu_K\cos(\phi - vt) - \mu_K'\cos(\phi + vt), \quad (5)$$

where L_0 is a scale for the momentum and the real coefficients $a_K, \varepsilon_K, \mu_K, \mu_K'$ have units of energy. The Hamiltonian is periodic in time with period $T = 2\pi/v$. If we choose a moment of inertia I that gives $a_K = L_0^2/I$, the Hamiltonian is similar to a rotor and with small L, the term $a_K\left(1 - \cos\left(\frac{L}{L_0}\right)\right) \approx \frac{L^2}{2I}$ is equal to the rotor's rotational kinetic energy.

We define a dimensionless momentum $p = L/L_0$ and adopt a dimensionless variable for time $\tau = vt$. Henceforth we work with time in units of the perturbation frequency v. The Hamiltonian for the perturbed Harper model

$$H(\phi,p,\tau)_{\text{PH}} = H_0(\phi,p) + H_1(\phi,\tau)$$
$$H_0(\phi,p) = a(1 - \cos p) - \varepsilon\cos(\phi)$$
$$H_1(\phi,\tau) = -\mu\cos(\phi - \tau) - \mu'\cos(\phi + \tau). \quad (6)$$

The equations of motion given by Hamilton's equations are consistent with those of equation 5, with dimensionless parameters,

$$a = \frac{a_K}{L_0 v}, \qquad \varepsilon = \frac{\varepsilon_K}{L_0 v}, \qquad \mu = \frac{\mu_K}{L_0 v}, \qquad \mu' = \frac{\mu_K'}{L_0 v}. \quad (7)$$

Phase space now consists of the torus with $\phi, p \in [0, 2\pi)$.

For the unperturbed system (with $\mu = \mu' = 0$), the frequency of libration around the stable fixed point at $p = 0, \phi = 0$ is $\omega_0 = \sqrt{\varepsilon a}$.

For $a, \varepsilon > 0$ the maximum and minimum energy of the unperturbed system are $2a + \varepsilon$ and $-\varepsilon$. As is true for the pendulum, given an energy, the orbit $\phi(\tau), p(\tau)$ of the unperturbed system can be written explicitly in terms of elliptic functions, however we have not found concise expressions for them.

Using Hamilton's equations, the fixed points of the unperturbed Harper system given by H_0 (in equation 6) are at $(\phi^*, p*) = (0,0), (0,\pi), (\pi,0), (\pi,\pi)$. Table I lists these fixed points their energies and whether they are stable or hyperbolic.

In each of Figures 1a, 3 and 3, we show a surface of section constructed from integrations of 200 different orbits of
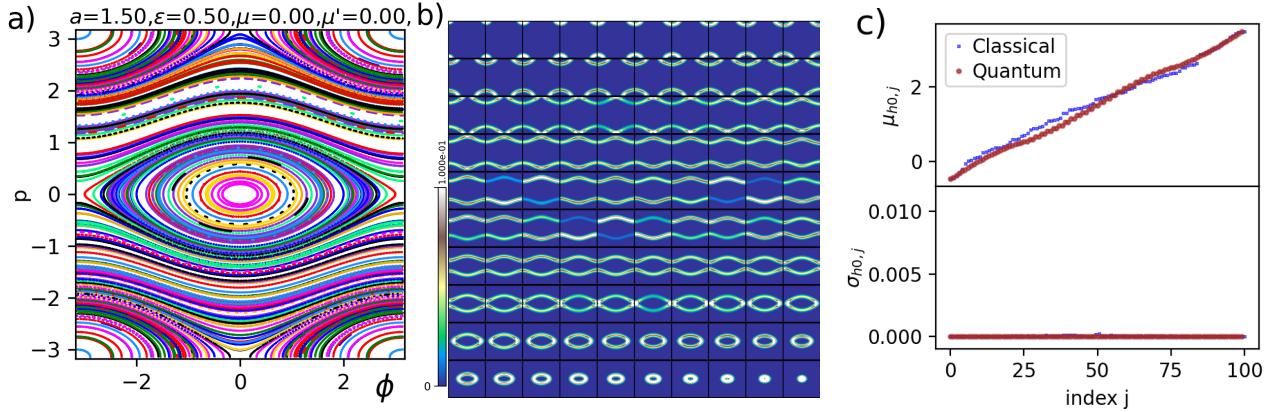
FIG. 1. a) We show a surface of section for regular (not chaotic) classical system, the Harper model with Hamiltonian in equation 6), and with parameters of the model printed on top of the figure. Points are plotted once every perturbation period of 2π. Each orbit is plotted with the same color points, and we choose different colors for different orbits. This particular system has $\mu = \mu' = 0$ and lacks sinusoidal time-dependent perturbations, but the figures are made in the same way as subsequent figures that have periodic perturbations. b) The related quantum model (with the same parameters $a, \varepsilon, \mu, \mu'$ as the classical one) has Hamiltonian operator in equation 15 and Floquet propagator given in equation 25. We show Husimi distributions for the eigenstates of the unitary propagator for the discrete quantized model with $N = 100$. Eigenstates of the propagator are arranged in order of their expectation value $\mu_{h0,j} = \langle \hat{h}_0 \rangle$. c) The top panel shows with solid brown dots the expectation value of the unperturbed Hamiltonian $\hat{h}_0$ for each eigenstate of the Floquet propagator. The mean values of the unperturbed Hamiltonian $\mu_{h0,j} = \langle H_0 \rangle$ are also computed for classically integrated orbits and these are shown as blue squares. The x-axis shows the state index j denoted a state for the quantum system, but the classical values are plotted over the same range in order of increasing mean value $\langle H_0 \rangle$, averaged from points in an orbit. The bottom panel shows (with brown dots) the standard deviations $\sigma_{h0,j}$ (equation 46) of the eigenvectors of the propagator. The standard deviation of the unperturbed Hamiltonian function for the same classical orbits as plotted in the top panel are plotted as blue squares.

TABLE I. Fixed points of the Harper model

(ϕ^*, p^*)	E	type
$(0,0)$	$-\varepsilon$	stable
(π, π)	$2a + \varepsilon$	stable
$(\pi, 0)$	ε	hyperbolic
$(0, \pi)$	$2a - \varepsilon$	hyperbolic

the Hamiltonian of equation 6. Initial conditions for the orbits are randomly chosen from uniform distributions covering phase space. Each orbit is plotted in one of 10 different colors and contains 500 points, with a point plotted each period (at $\tau = 0$ modulo 2π). In Figure 1, the classical Hamiltonian is regular in the sense that each orbit is quasiperiodic or a curve (also called a torus when referring to a surface in a higher dimensional space that is filled by the trajectory). In Figures 2a and 3a, the parameters $a, \varepsilon, \mu, \mu'$ are chosen to show one or more area filling chaotic regions that separate regions containing quasi-periodic orbits.

When $a = \varepsilon$, there is a single separatrix energy, associated with the energy at the hyperbolic fixed points (listed in Table I) and the separatrix forms a diamond along trajectories $p(\phi)_s = \pm\phi \pm \pi$. When $a \neq \varepsilon$ there are two separatrix energies E_s associated with separate orbits

$$
\begin{aligned}
\cos \frac{p_s(\phi)}{2} &= \pm\sqrt{\frac{\varepsilon}{a}} \sin \frac{\phi}{2} \quad \text{for} \quad E_s = 2a - \varepsilon \\
\sin \frac{p_s(\phi)}{2} &= \pm\sqrt{\frac{\varepsilon}{a}} \cos \frac{\phi}{2} \quad \text{for} \quad E_s = \varepsilon.
\end{aligned}
\tag{8}
$$

These orbits divide the regions of phase space in the model shown in Figure 1a. The separatrix orbits are the regions that

become ergodic under perturbation as illustrated in Figure 2a and 3a.

II. A QUANTUM MECHANICAL VERSION OF THE PERTURBED HARPER MODEL

We consider the classical Hamiltonian of equation 6. To facilitate calculation associated quantum system, we choose to work in a discrete rather than continuous quantum space. We approximate the system with an N dimensional quantum space (an N dimensional normed complex vector space). We choose a set of orthonormal basis states labelled with integers; $|j\rangle$ for $j \in \mathbb{Z}_N$ where $\mathbb{Z}_N$ is the set of integers $\{0, 1, ..., N-1\}$. The operator associated with measurement of the angle ϕ we associate with this basis

$$
\hat{\phi} = \sum_{j=0}^{N-1} \frac{2\pi j}{N} |j\rangle \langle j|.
\tag{9}
$$

Because the classical system of equation 6 is also periodic in p, we simultaneously quantize the momentum p. In the limit of large N, we should recover the behavior of a quantum system in a continuous Hilbert space with angle $\phi \in [0, 2\pi)$ and periodic.

Two bases are mutually unbiased if every measurement outcome is equally probable when a system in a state that is a basis element in one basis is measured with an operator that is diagonal in the other basis (e.g., Wootters[62]). In the infinite dimensional case, position and momentum operators, $\hat{q}, \hat{p}$ are associated with two bases that are mutually unbiased and
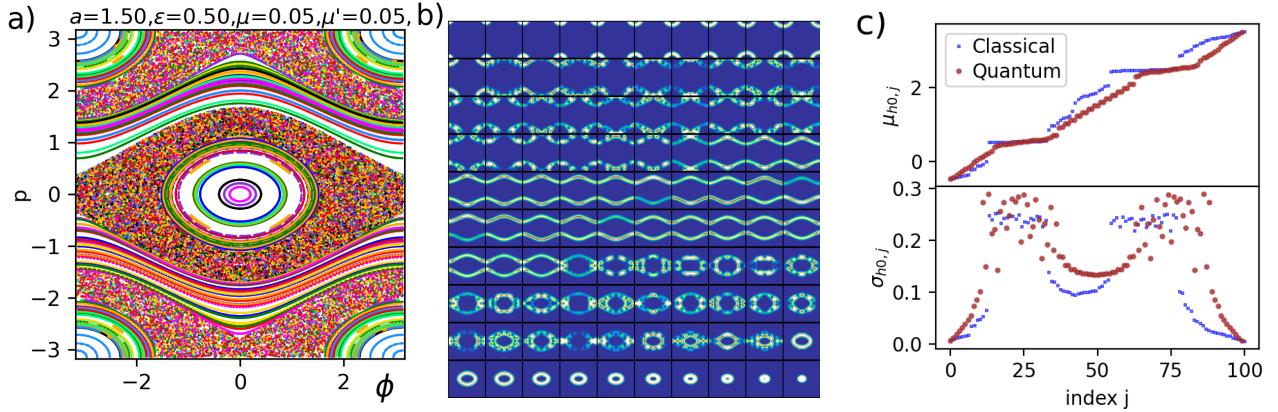
FIG. 2. a) Similar to Figure 1a except for a classical system that has chaotic regions. The parameters $a, \varepsilon, \mu, \mu'$ of the Hamiltonian are printed on the top left. b) We show the Hussimi distributions of the Floquet eigenstates of the associated quantum model with $N = 100$. The Hussimi distributions of some eigenstates of the Floquet propagator fill the chaotic regions in phase space seen in the associated classical system. The quantum system has $N = 100$ states. c) Similar to Figure 1c. We show energy means and dispersions from both classical orbits and Floquet eigenstates. Chaotic eigenstates have large standard deviations $\sigma_{h0,j}$ (defined in equation 46). Chaotic orbits also have large energy standard deviations.

related by Fourier transform. Given a particular orthonormal basis in a discrete quantum system, the discrete Fourier transform can be used to generate a second basis that is a mutually unbiased basis with respect to the first, and we use that basis to construct the momentum operator $\hat{p}$. In an orthonormal basis $\{|n\rangle\} : n \in \mathbb{Z}_N$ for an N dimensional discrete quantum space, the discrete Fourier transform

$$\hat{Q}_{FT} = \frac{1}{\sqrt{N}} \sum_{j,k=0}^{N-1} \omega^{jk} |j\rangle \langle k|, \qquad (10)$$

with

$$\omega \equiv e^{2\pi i/N}. \qquad (11)$$

Using the discrete Fourier transform, we construct an orthonormal basis consisting of states

$$|m\rangle_F = \hat{Q}_{FT} |m\rangle = \frac{1}{\sqrt{N}} \sum_{j=0}^{N-1} \omega^{mj} |j\rangle \qquad (12)$$

with $m \in \mathbb{Z}_N$. Because

$$\langle j|m\rangle_F = \frac{\omega^{jm}}{\sqrt{N}}. \qquad (13)$$

has amplitude equal to $1/\sqrt{N}$, independent of j, m, the basis $\{|k\rangle_F\} : k \in \mathbb{Z}_N$ is mutually unbiased with respect to the basis $\{|n\rangle\} : n \in \mathbb{Z}_N$.

Because both $p, \phi \in [0, 2\pi)$ and are both periodic in the classical Hamiltonian of equation 6, an operator for momentum, similar to that for the angle $\hat{\phi}$ (equation 9), can be defined in the Fourier basis

$$\hat{p} = \sum_{m=0}^{N-1} \frac{2\pi m}{N} |m\rangle_F \langle m|_F. \qquad (14)$$

With both dimensionless momentum and angle operators $\hat{p}, \hat{\phi}$ (equations 9, 14) defined in a discrete quantum space, the Hamiltonian of equation 6 be written in terms of these operators

$$\hat{h}(\tau)_{\mathrm{PH}} = \hat{h}_0(\hat{p}, \hat{\phi}) + \hat{h}_1(\hat{\phi}, \tau)$$
$$\hat{h}_0(\hat{\phi}, \hat{p}) = a(1 - \cos \hat{p}) - \varepsilon \cos \hat{\phi}$$
$$\hat{h}_1(\hat{\phi}, \tau) = -\mu \cos(\hat{\phi} - \tau) - \mu' \cos(\hat{\phi} + \tau). \qquad (15)$$

The operators $\hat{p}, \hat{\phi}$ don't commute, but because our Hamiltonian is separable, with kinetic energy term only a function of $\hat{p}$ and potential energy term only a function of $\hat{\phi}$, we don't need to consider the order of these two operators during quantization. The eigenvalues of $\hat{p}$ and $\hat{\phi}$ are real but exhibit a jump of 2π between $|0\rangle$ and $|N-1\rangle$ states and between $|0\rangle_F$ and $|N-1\rangle_F$ states, respectively. However, the jump in the eigenvalues of $\hat{\phi}$ and $\hat{p}$ does not affect the Hamiltonian operator of the Harper model because it is periodic in both operators.

To summarize, we quantize a periodic classical system that is described by a separable Hamiltonian in the following way that is similar to that used to study quantum systems on the torus (e.g., Saraceno[45]). We choose a classical system with a Hamiltonian function that is a sum of a potential energy term that is a function of the canonical angle coordinate and a kinetic energy term that is a function of the momentum. We restrict the phase space of the classical system so that it is doubly periodic. We select a discrete quantum space and create an operator for angle based on a basis labelled with integers. We use the discrete Fourier transform to construct a Fourier basis and momentum operator that is diagonal in the Fourier basis. The Hamiltonian is converted to an operator using the position and momentum operators in the discrete quantum space. This procedure gives us a map ϕ_N, dependent upon positive integer N, from a classical doubly periodic and separable Hermitian operator (our classical Hamiltonian). Below in section II E we show how our quantization map is often equivalent to

that generated via a Wigner-Weyl transformation.

For the perturbed Harper model, the map between classical Hamiltonian and quantum operator is

$$H(\phi, p, t)_{PH} \underset{\phi_N}{\longrightarrow} \hat{h}(\hat{\phi}, \hat{p}, t)_{PH} \quad (16)$$

with dimensionless classical Hamiltonian of equation 6 on the left and the dimensionless Hermitian operator of equation 15 on the right.

Because the discrete Fourier transform gives the basis of our momentum operator, phase space contains N states in both momentum and coordinate angle bases. The discrete quantum space facilitates computation of quasi-energy levels and eigenstates as we can compute them using matrix operations, aiding in potential applications on systems that are finite dimensional, such as quantum computers.

A. Domain size and Planck's constant

While classical equations of motion use Hamilton's equations to generate the dynamics, in a quantum system with Hamiltonian $\hat{H}$, the time dependence $\partial_t = -\frac{i}{\hbar}\hat{H}$ and is inversely proportional to the reduced Planck's constant $\hbar$. From the dimensionless operator in Equation 15, we can construct a Hamiltonian operator with units of energy (and matching the classical Hamiltonian K_{PH} of equation 5) is

$$\hat{k}_{PH} = E_0 \hat{h}_{PH}, \quad (17)$$

with $E_0 = L_0 \nu$.

We apply the Bohr-Sommerfeld quantization condition $\int p dq = 2\pi N \hbar$ (e.g., following Wei and Arovas[59] for the kicked quantum Harper model) where N is a positive integer which we set to the dimension of our discrete quantum vector space. For our classical system, the momentum p has units of angular momentum so the Bohr-Sommerfeld quantization condition is $\int L d\phi = 2\pi n\hbar$. The left hand size is the domain size in the phase space of our system which is equal to $(2\pi)^2 L_0$. The Bohr-Sommerfeld quantization condition gives

$$\frac{L_0}{\hbar} = \frac{N}{2\pi}. \quad (18)$$

With this prescription, the dimension of the discrete quantum space N is related to the domain momentum size in units of $\hbar$. Equivalently if we choose L_0 and N, then $\hbar$ assumes a particular value.

Equation 18 implies that in the large N limit, at a fixed value for $\hbar$, the size of the domain $L_0 \to \infty$ and we would recover the perturbed pendulum model of equation 1. We can also take the large N limit at a fixed domain size L_0, which means that $\hbar \to 0$, and is equivalent to the semi-classical limit. Note $E_0 = \frac{N}{2\pi}\hbar\nu$. Again taking E_0 fixed, $N \to \infty$ is equivalent to the classical limit $\hbar \to 0$. Alternatively, $N \to \infty$ with $\hbar$ fixed gives $E_0 \to \infty$.

The sensitivity of possible parameter values to $\hbar$ (and vice versa) when approximated on a discrete quantum space also occurs with quantizations of the kicked rotor (e.g.,

Chirikov et al. [16]) and the kicked Harper model (e.g., Wei and Arovas[59]).

With the domain size in momentum spanning $[0, 2\pi L_0]$, the operator $\hat{p} = \frac{\hat{L}}{L_0}$. Using equation 18 the operator

$$\hat{L} = \sum_m \frac{2\pi m}{N} L_0 |m\rangle \langle m| = \sum_m \hbar m |m\rangle \langle m|, \quad (19)$$

as expected. Thus equation 15 can also be written

$$\hat{h}_{PH} = a \left(1 - \cos \frac{\hat{L}}{L_0} \right) - \varepsilon \cos \hat{\phi}$$
$$- \mu \cos(\hat{\phi} - \tau) - \mu' \cos(\hat{\phi} + \tau). \quad (20)$$

For every classical system in the dimensionless form of equation 6 we can associate a quantum system in the form of equation 15. To choose a discrete quantum system we must choose N, which via equation 18 sets $L_0/\hbar = N/(2\pi)$ and $E_0/\hbar = L_0\nu/\hbar = \nu N/(2\pi)$.

With $a, \varepsilon > 0$, the maximum energy $E_0(2a + \varepsilon)$ and the minimum energy is $-E_0\varepsilon$. With N energy levels, the distance between the energy levels is about $\delta E \sim 2E_0(\varepsilon + a)/N$.

Time evolution depends on the operator

$$\frac{\hat{k}_{PH}(t)}{\hbar} = \frac{L_0 \nu \hat{h}_{PH}(\tau)}{\hbar} = \frac{N}{2\pi} \nu \hat{h}_{PH}(\tau) \quad (21)$$

using equation 18 and with $\tau = \nu t$. The above relation also implies

$$\frac{\hat{k}_{PH} T}{\hbar} = N \hat{h}_{PH} \quad (22)$$

which is relevant when computing the propagator for evolution over a duration equal to the perturbation period.

The choice of a discrete quantum space facilitates numerical computation of the Floquet operator over the time $T = 2\pi/\nu$,

$$\hat{U}_T = \mathcal{T} e^{-\frac{i}{\hbar} \int_0^T \hat{k}(\nu t)_{PH} dt} \quad (23)$$

where $\mathcal{T}$ indicates a product of time-ordered unitary operators computed in the limit of small step size. With n_t the number steps, and $dt = T/n_t$,

$$\hat{U}_T = \lim_{n_j \to \infty} \mathcal{T} \prod_{j=0}^{n_j - 1} e^{-\frac{i}{\hbar} \hat{k}_{PH}(jdt) \, dt}. \quad (24)$$

Using equation 18 the Floquet propagator in terms of our rescaled Hamiltonian operator $\hat{h}_{PH}$ (of equation 15) is

$$\hat{U}_T = \mathcal{T} e^{-\frac{i}{\tilde{h}} \int_0^{2\pi} \hat{h}(\tau)_{PH} d\tau} \quad (25)$$

with

$$\tilde{h} = \frac{2\pi}{N} \quad (26)$$

acting like $\hbar$ in our rescaled system. Planck's constant is similarly rescaled when quantizing the kicked rotor[16]. The unitary

operator $\hat{U}_T$ describes the evolution of our rescaled quantum system from dimensionless time $\tau = 0$ to 2π.

Parameters describing the quantum system (equation 15) include those chosen for the associated classical system (equation 6); $a, \varepsilon, \mu, \mu'$, also listed in equation 7. In addition to those, we also choose the dimension N of the associated discrete quantum space which in turn sets the dimensionless ratio $L_0/\hbar$.

B. Computing the propagator via Suzuki-Trotter decomposition

We numerically compute the unitary transformation of the Floquet fpropagator $\hat{U}_T$ in equation 25 via Suzuki-Trotter decomposition (e.g., Hatano and Suzuki [23]). The Hamiltonian is divided into two pieces, one that contains the momentum operator and the other that contains the angle operator,

$$\hat{h}(\tau)_{\text{PH}} = \hat{A}_p + \hat{B}_\phi(\tau) \tag{27}$$

with

$$\hat{A}_p = a(1 - \cos \hat{p})$$
$$= \sum_{m=0}^{N-1} a\left(1 - \cos\frac{2\pi m}{N}\right)|m\rangle_F \langle m|_F \tag{28}$$

$$\hat{B}_\phi(\tau) = -\varepsilon \cos\hat{\phi} - \mu\cos(\hat{\phi} - \tau) - \mu'\cos(\hat{\phi} + \tau)$$
$$= \sum_{j=0}^{N-1}\left[-\varepsilon\cos\frac{2\pi j}{N} - \mu\cos\left(\frac{2\pi j}{N} - \tau\right)\right.$$
$$\left. -\mu'\cos\left(\frac{2\pi j}{N} + \tau\right)\right]|j\rangle\langle j|. \tag{29}$$

We approximate unitary evolution of a duration $d\tau$ with the approximation for an exponential of two operators $\hat{A}, \hat{B}$ with a symmetric second order decomposition

$$e^{(\hat{A}+\hat{B})d\tau} \approx e^{\frac{\hat{A}d\tau}{2}} e^{\hat{B}d\tau} e^{\frac{\hat{A}d\tau}{2}} + \mathcal{O}(d\tau^3) + ... \tag{30}$$

We approximate the propagator in equation 25, with evolution from $\tau = 0$ to 2π (a period), using n_τ steps of duration $d\tau = 2\pi/n_\tau$

$$\hat{U}_T \approx \Lambda_A^{\frac{1}{2}}\left(\mathcal{T}\prod_{j=0}^{n_\tau - 1}\Lambda_{B,j}\Lambda_A\right)\Lambda_A^{-\frac{1}{2}} \tag{31}$$

with operators

$$\Lambda_A = e^{-\frac{iN}{n_\tau}\hat{A}_p}$$
$$\Lambda_{B,j} = e^{-\frac{iN}{n_\tau}\hat{B}_p\left(\frac{2\pi j}{n_\tau}\right)} \tag{32}$$

with $\hat{A}_p, \hat{B}_\phi$ from equations 28 and 29. Using this approximation, we numerically compute propagators for systems with different parameters and in different dimensions N. Because of the factor of N in the argument of of $\hat{U}_T$, we use $n_\tau = 5N$

Trotterization steps though we did not see significant differences between the properties of propagators computed with a few times fewer or greater numbers of steps. After we have numerically computed a propagator matrix, we compute its associated eigenvectors and eigenvalues or quasi-energies with standard linear algebra computational algorithms.

C. Discrete operators

The position operator $\hat{\phi}$ is a diagonal operator in the $\{|j\rangle\}$ basis and the momentum operator $\hat{p}$ is a diagonal operator in the Fourier basis; $\{|m\rangle_F\}$. In analogy to a continuous system, we use two discrete operators, one corresponding to a translation in momentum, and the other giving a translation in real space, to generate a displacement operator. In analogy with coherent states for a continuous system, discrete coherent states are created via operating with the displacement operator on a minimum uncertainty state that resembles a Gaussian.

The unitary $\hat{Z}, \hat{X}$ operators, introduced by Schwinger in his work on mutually unbiased bases[47], (also see Björk et al.[6])

$$\hat{Z} = \sum_{n=0}^{N-1}\omega^n |n\rangle\langle n| = \sum_{k=0}^{N-1}|k+1\rangle_F\langle k|_F \tag{33}$$

$$\hat{X} = \sum_{k=0}^{N-1}\omega^{-k}|k\rangle_F\langle k|_F = \sum_{n=0}^{N-1}|n+1\rangle\langle n|. \tag{34}$$

In these expressions, addition for the state vectors is modulo N. These are equivalent to a set of generalized Pauli matrices called *clock and shift operators* or Weyl-Heisenberg matrices[2]. These describe shifts in a periodic discrete quantum space. These operators have been used to study the quantized Baker map on the torus, and in phase space[3] and in quantum information theory (e.g., Björk et al.[6]).

D. Husimi distributions constructed from discrete coherent state analogs

To compare the quantum and classical systems, we compute Husimi distributions (also called the Husimi Q representation) which are quantum analogs to classical phase space distributions[12]. Our procedure for constructing Husimi distributions on a torus (a doubly periodic space) uses a discrete displacement operator, following[3,6,20,41,42,45]. The displacement operator is used to construct discrete analogs for coherent states which in turn are used to compute Husimi distributions.

A displacement operator is

$$\hat{D}(k,l) = \omega^{-kl/2}\hat{Z}^k\hat{X}^l. \tag{35}$$

for integers $k, l \in \{0, 1, ..., N-1\}$. Because $\hat{X}$ acts like a raising operator in the $|n\rangle$ basis and $\hat{Z}$ acts like a raising operator in the $|k\rangle_F$ basis, the displacement operator $D(k,l)$ translates in position and momentum.
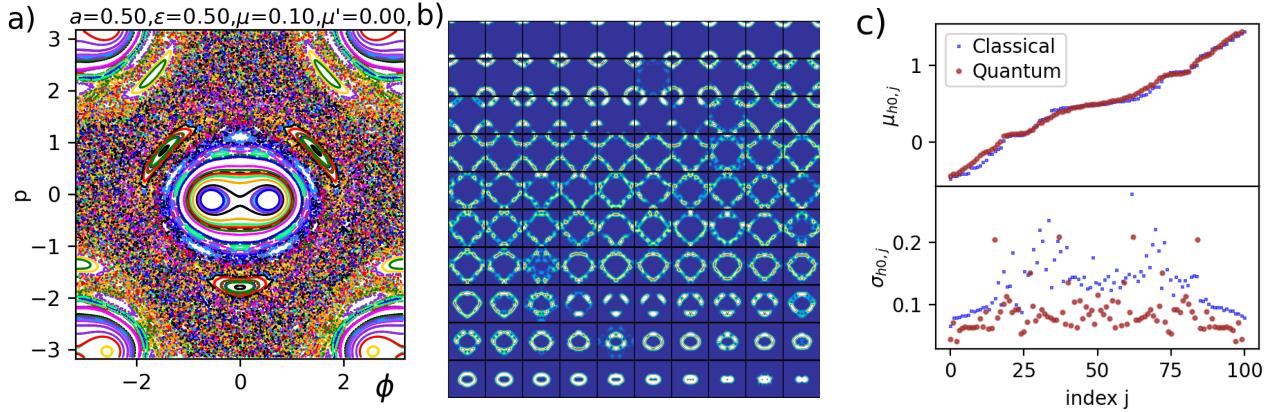
FIG. 3. Similar to Figure 2 except for a classical system that has larger chaotic regions and has an asymmetric perturbation; $\mu \neq \mu'$. This system also has $N = 100$ states.
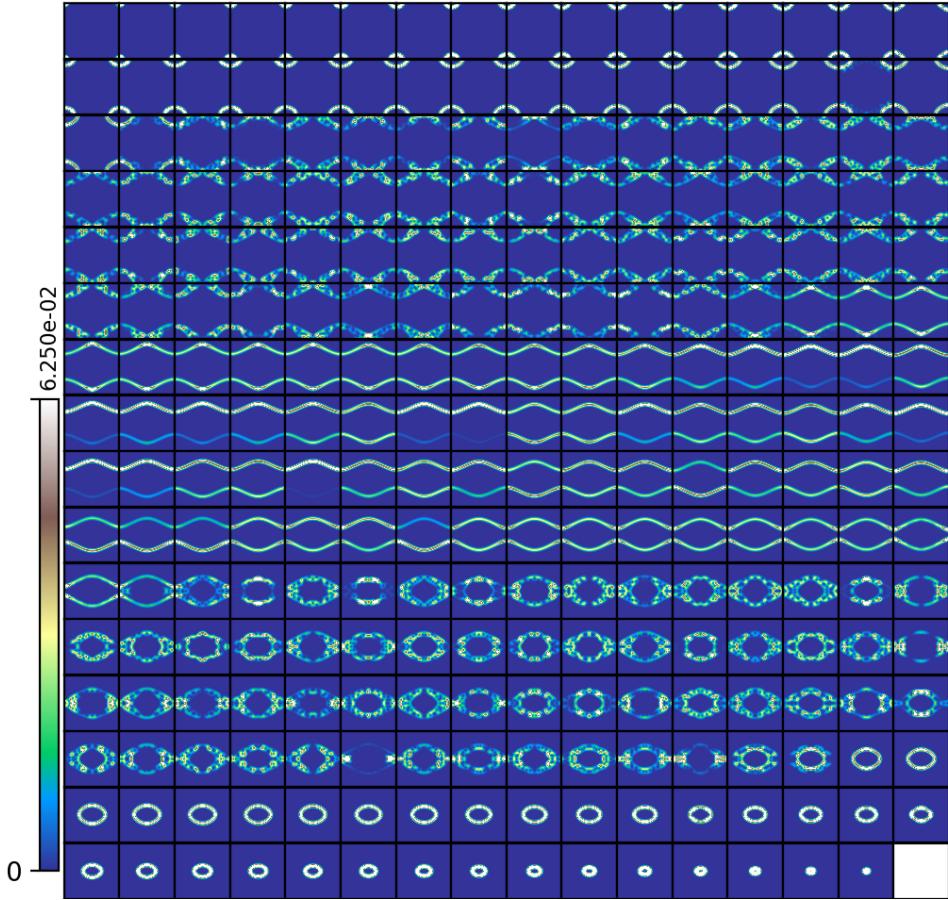

FIG. 4. Similar to Figure 2b except that the number of states $N = 255$ instead of 100. The Hamiltonian has the same parameters $a, \varepsilon, \mu, \mu'$ as the system shown in Figure 2. The Husimi distributions are similar with larger N, though there may be additional localized states located with the chaotic region.

Following Galetti and Marchiolli[20], to generate coherent state analogs, we start with a unimodal eigenstate of the discrete Fourier transform

$$|\tilde{\eta}\rangle = b_\eta \sum_{m=0}^{N-1} \vartheta_3 \left(\frac{\pi m}{N}, e^{-\pi/N} \right) |m\rangle$$

$$\propto \sum_{m=0}^{N-1} \sum_{j=-\infty}^{\infty} e^{-\frac{\pi}{N}(m+jN)^2} |m\rangle . \tag{36}$$

Here ϑ_3 is a Jacobi theta function and the coefficient $b_\eta \approx \left(\frac{2}{N}\right)^{\frac{1}{4}}$ serves to normalize the state vector. In the limit of large N, this becomes a Gaussian function which is the state vector with the minimum possible uncertainty in phase space.

Because the state $|\tilde{\eta}\rangle$ is equal to its Fourier transform and resembles a Gaussian, it acts like a state of optimal uncertainty (like a Gaussian function in the continuous setting). The expectation value

$$\langle \tilde{\eta} | f(\hat{X}) | \tilde{\eta} \rangle = \langle \tilde{\eta} | f(\hat{Z}) | \tilde{\eta} \rangle$$

for any polynomial function $f()$, because $\hat{Z} = \hat{Q}_{FT} \hat{X} \hat{Q}_{FT}^\dagger$ and $\hat{Q}_{FT} | \tilde{\eta} \rangle = | \tilde{\eta} \rangle$. So $\langle \hat{X}^2 \rangle = \langle \hat{Z}^2 \rangle$ for the state $| \tilde{\eta} \rangle$.

We compute discrete analogs for coherent states using the displacement operator of equation 35 and the state $|\tilde{\eta}\rangle$ (defined in equation 36)

$$|k,l\rangle = \hat{D}(k,l) | \tilde{\eta} \rangle \tag{37}$$

for each $k,l \in \{0,....,N-1\}$. We compute the Husimi function of a state vector $|\psi\rangle$

$$H_Q(k,l) = | \langle \psi | k,l \rangle |^2. \tag{38}$$

By computing H_Q for $k,l \in \{0,1,....,N-1\}$ we produce an $N \times N$ grid of positive values representing the phase space distribution of the state $|\psi\rangle$.

E. Wigner-Weyl quantization

The way we quantized the perturbed Harper model, taking $H \to \hat{h}$ described at the beginning of section II, is equivalent to quantization via a discrete Weyl symbol or (also called a discrete Wigner-Weyl transform), (e.g., Wootters[61]). Following Björk et al.[6], a point operator $\hat{A}_{nk}$ for a discrete system can be constructed from the displacement operator that resembles the Wigner-Weyl transform of a continuous system;

$$\hat{A}_{nk} = \frac{1}{N} \sum_{x=0}^{N-1} |n+x\rangle \langle n-x| \omega^{2xk} \tag{39}$$

$$= \frac{1}{N} \hat{X}^n \hat{Z}^k \hat{P} \hat{Z}^{-k} \hat{X}^{-n}$$

$$= \frac{1}{N} \hat{D}(k,n) \hat{P} \hat{D}(k,n)^\dagger. \tag{40}$$

for integers $n,k \in \{0,1,....N-1\}$ and with parity operator

$$\hat{P} = \sum_{x=0}^{N-1} |x\rangle \langle -x \mod N|. \tag{41}$$

The Weyl transform of a function of discrete phase space denoted with integers $a(k,n)$ gives an operator

$$\hat{a} = \sum_{k,n=0}^{N-1} a(k,n) \hat{A}_{nk}. \tag{42}$$

Only if N is odd does $\hat{A}_{nk}$ gives a basis for operators w.r.t to the Frobenius or Hilbert-Schmidt norm;

$$\text{tr}\left(A_{nk}^\dagger A_{n'k'}\right) = \delta_{n,n'} \delta_{k,k'} \text{ iff } N \text{ odd.} \tag{43}$$

The following sums are valid for N odd;

$$\sum_{k=0}^{N-1} \hat{A}_{nk} = \sum_{x=0}^{N-1} |n+x\rangle \langle n-x| \sum_{k=0}^{N-1} \omega^{2kx} \frac{1}{N} = |n\rangle \langle n|$$

$$\sum_{n=0}^{N-1} \hat{A}_{nk} = |k\rangle_F \langle k|_F \tag{44}$$

so the first index of the point operator $\hat{A}_{nk}$ is a coordinate index and the second index is a momentum index.

Using $v(n,k) = V(n)$ corresponding to a potential energy function, we use equations 40 - 44 to create the operator $\hat{v} = \sum_n V(n) |n\rangle \langle n|$ using the Wigner-Weyl transform. With $t(n,k) = T(k)$ corresponding to a potential energy function in the discrete space, we find that $\hat{t} = \sum_k T(k) |k\rangle_F \langle k|_F$ in the Fourier basis. Thus Weyl quantization of the separable Hamiltonian such as that in equation 6 with $T(k) = a(1 - \cos(2\pi k/N))$ gives the same Hamiltonian operator as in equation 15, but only for odd N discrete dimension. Leonhardt[30] showed how to create a well-behaved discrete point operator (with $2N \times 2N$ points) if the dimension N is even.

Quantization of a separable Hamiltonian using a pair of mutually unbiased bases, discussed in section II, and the discrete coherent states for constructing Husimi distributions, (discussed in section II D) can be done for dimension N either even or odd. However Weyl quantization via the same point operator used to make coherent states is only equivalent to quantization via levering a pair of mutually unbiased bases if dimension N is odd.

III. NUMERICAL COMPUTATIONS

Using the procedure for Suzuki-Trotter decomposition described in section II B, we compute the propagator $\hat{U}_T$ for some quantized periodically perturbed Harper models (with Hamiltonian of equation 15) and compare them to their associated classical model (with Hamiltonian of equation 6). Three different model systems are shown in Figures 1 – 3. We show orbits of the associated classical model in the a) panels, and in the b) panels we show Husimi distributions, computed as described in section II D, for the eigenvectors, also called Floquet states, of the propagator $\hat{U}_T$. The center of the a) subfigures is the origin $(\phi, p) = (0,0)$. Each panel in the b) subfigure shows an $N \times N$ array computed with a single eigenstate of the Floquet propgator $\hat{U}_T$. Each pixel of a panel has different indices k,l setting the coherent state for computing equation 38, and with the central value in the image corresponding has indices $k,l = 0$ so as to match the $(\phi, p) = (0,0)$ central position of the classical phase space surfaces of section. This makes it possible to visually compare the classical phase space surfaces of sections in the a) subfigure to the Husimi distributions in the b) subfigure. In Figures 1, 2 and 3, the dimension of the

quantum system $N = 100$. The Husimi distributions shown in Figure 4 have the same parameters $a, \varepsilon, \mu, \mu'$ as the system shown in Figure 2 but the dimension is larger, $N = 255$. The Husimi distributions are displayed with a maximum level of $1/\sqrt{N}$ and a colorbar is included on the left sides of Figure 1b and Figure 4. In Figures 2b and 3b, with dimension $N = 100$, the colorbar is the same as shown in Figure 1b.

A comparison between the Husimi distributions and the classical orbits seen in the surfaces of section illustrates that the eigenstates of the quantized models are closely related to the orbits of the classical system. For the systems shown in Figures 2 and 3 the phase space regions containing area filling chaotic classical orbits, have Husimi distributions that are wider and cover the chaotic region.

A. An order for the eigenstates of the Floquet propagator

The Floquet propagator, $\hat{U}_T$ (equation 25), because it is unitary, has complex eigenvalues of magnitude 1. An eigenvalue of $\hat{U}_T$ in the form $e^{i\lambda}$ can be described by its argument or phase, real λ, which is called a quasi-energy. We find that the Husimi distributions of the eigenvectors of $\hat{U}_T$ appear to be in a random order if we sort them in order of increasing quasi-energy. Instead, we sort the eigenstates of $\hat{U}_T$ in order of their expectation value of the unperturbed and static portion of the Hamiltonian, $\hat{h}_0$ (specified in equation 15). For each eigenstate $|w_j\rangle$ (indexed by j) of $\hat{U}_T$, we compute the expectation value

$$\mu_{h0,j} \equiv \langle w_j | \hat{h}_0 | w_j \rangle. \tag{45}$$

Figures 1b, 2b, and 3b show the Husimi distributions for the eigenstates of $\hat{U}_T$ in consecutive order of expectation value $\mu_{h0,j}$. We find that the Husimi distribution of an eigenstate $|w_j\rangle$ of the Floquet propagator $\hat{U}_T$ resembles classical orbits of the associated classical system with energy near $\langle w_j | \hat{h}_0 | w_j \rangle$.

B. Energy dispersions and ergodicity

In the top panels of Figures 1c, 2c, and 3c we plot with brown dots the expectation $\mu_{h0,j}$ of the unperturbed Hamiltonian $\hat{h}_0$ for each eigenstate $|w_j\rangle$ of the Floquet propagator $\hat{U}_T$. In the bottom panels we plot the standard deviation $\sigma_{h0,j}$ for each Floquet eigenstate, where

$$\sigma_{h0,j} = \sqrt{\langle w_j | \hat{h}_0^2 | w_j \rangle - (\langle w_j | \hat{h}_0 | w_k \rangle)^2}. \tag{46}$$

The means and standard deviations are plotted as a function of index j after putting the states in order of increasing $\mu_{h0,j}$. Figures 2c, and 3c show that where classical orbits are chaotic, area filling, and exhibit variations in the energy of the unperturbed Hamiltonian function, the quantum eigenstates have a higher standard deviation $\sigma_{h0,j}$. For our perturbed Harper system, the standard deviation $\sigma_{h0,j}$, computed from the eigenstates of the Floquet propagator, measures of the width (in energy) of the chaotic region.

In Figures 1c, 2c, and 3c and for their associated classical Hamiltonian, we integrate for 400 periods, giving a series of 400 points (each separated in time by a period) in phase space, for each of 500 orbits. The initial conditions for these 500 orbits are randomly chosen from a uniform distribution that covers phase space. The 400 phase space positions from each orbit give a series of values for the energy $H_0(\phi, p)$, the value of the classical Hamiltonian. The mean μ_{H0} and standard deviation σ_{H0} for the unperturbed Hamiltonian function $H_0(p, \phi)$ are then computed from the points in each orbit. The orbits are sorted in order of their mean energy, μ_{H0}, and these mean values shown in Figures 1c – 3c top panel with blue squares. The bottom panel in Figure 1c – 3c shows the standard deviations σ_{H0} computed from the same orbits. While the horizontal axis on this plot is given with respect to the index of the sorted eigenstates of the quantum system, we have displayed the classically computed energy means and standard deviations so as to cover the same horizontal range. We don't expect the quantum means and standard deviations to exactly match the classical ones because the classical orbit initial conditions were randomly chosen. Figures 2c, and 3c illustrate that the means and standard deviations of the unperturbed Hamiltonian classically computed from the orbits are similar to the means and standard deviations computed from the from eigenstates of the associated quantum model. The similarity between quantum and classical energy dispersions suggests that the dispersion of the unperturbed energy gives an quantitative estimate for ergodicity in both settings.

Figure 4 shows a quantum system identical to that shown in Figure 2b except that the number of states $N = 255$ instead of 100. The similarity of the Husimi function at $N = 255$ and $N = 100$ illustrates that the ergodicity is not reduced at larger N. In the $N = 255$ system, there is a localized eigenstate embedded within the chaotic zone (in about the middle of the third row from the top). This behavior is perhaps similar to the phenomena of quantum scars seen in billiard systems and near periodic classical orbits[4,24]. We chose an odd dimension for this system and checked that the properties of the Floquet eigenstates (such as the appearance of the Husimi distributions) are not strongly dependent upon whether the dimension N is even or odd.

In Figures 2c and 3c, the classical orbits within the chaotic region have similar average energy, (and had we integrated the orbits longer, the average could have approached a single value). The differences between energies of the Floquet eigenstates (computed via an expectation value of $\hat{h}_0$; equation 45) in this chaotic region are reduced. In the high N limit, corresponding to the classical limit, we expect that the differences between the energies of the Floquet eigenstates would be even smaller.

In a classical system, one notion of ergodicity is that the time average of an observable is equal to its spatial average. This notion was extended to quantum systems by Shnirel'man[51]. When the classical dynamics is ergodic, for almost all eigenstates, the expectation values of observables converges to the phase-space average in the limit the dimension of the quantum space goes to infinity, $N \to \infty$ (also see Kurlberg and Rudnick[27]).

The close correspondence between the energy dispersions computed from the classical orbits and the quantum equivalent computed from the eigenstates of the Floquet propagator (shown in in Figures 1c, 2c, and 3c) suggests that the dispersion of the unperturbed Hamiltonian (equation 46) gives a quantitative estimate for quantum ergodicity. For two systems with the same values of parameters $a, \varepsilon, \mu, \mu'$ but with two different dimensions N (Figures 2b and 4b) we find that the eigenstates of the Floquet operator that are within the classical chaotic region in phase space have similar high standard deviations $\sigma_{h0,j}$ in both cases. This suggests that these quantum systems would be ergodic in the sense of a high N limit, (following[27,51]. At larger N there could still be a small subset of eigenstates of the Floquet propagator within the chaotic regions, that are strongly localized or associated with periodic orbits, akin to quantum scars (e.g.,[4,24]).

To illustrate the notion of ergodicity in the quantum system, in Figure 5 we show a series of Husimi distributions for Hamiltonian models that have the same parameters except each one has a different value of N. From left to right, the dimension increases by a factor of 2 from panel to panel. Each Husimi distribution is constructed from an eigenstate of the Floquet propagator that has energy near the separatrix. We choose $a = \varepsilon$ so that there is only a single separatrix but set $\mu' \neq \mu$ so the model is lopsided like that shown in Figure 3. The separatrix region is chaotic and at larger N the eigenstates appear increasingly diffuse and evenly distributed. This suggests that in the high N limit regions that are chaotic in the classical system could correspond to an ergodic subspace that is ergodic in the sense defined by Shnirel'man[51].

C. The quasi-energy spacing distributions

Distributions of differences $s_j = \lambda_{j+1} - \lambda_j$ between consecutive quasi-energies, normalized by their mean value $\langle s \rangle$, are shown in Figure 6. In Figure 6a we show the quasi-energy spacing distributions for the classically regular (non-chaotic) model shown in Figure 1 as an orange filled histogram and that of the perturbed and chaotic system shown in Figure 3 as a purple hatched histogram. In Figure 6a, a magenta dotted line shows an exponential distribution, expected for a Poisson process, also normalized with a mean of 1. The dashed black line shows the Wigner-Dyson distribution

$$p_{\text{GOE}}(s) = \frac{\pi}{2} s e^{-\frac{4}{\pi} s^2} \tag{47}$$

which is that of level spacings for the Gaussian orthogonal ensemble (GOE) random matrix model, also normalized so that its mean is 1.

Figure 6a shows that the distribution of energy level spacings is sensitive to the presence of chaotic regions in the model, with the regular model exhibiting a distribution more similar to an exponential. The distribution for the system containing chaotic regions is broader and closer to that of a random matrix model.

Figures 2 and 4 show a classical system that has two chaotic regions. For this system but with $N = 999$, we divide the Floquet eigenstates into two sets, depending upon whether their standard deviation $\sigma_{h0,j}$ is above or below 0.18. Using these two subspaces, we separately compute two quasi-energy spacing distributions, and these are shown in Figure 6b. The distribution for eigenstates with $\sigma_{h0,j} < 0.18$ and associated with integrable regions in phase space in the associated classical model, is plotted as a filled pink histogram. The distribution for eigenstates with $\sigma_{h0,j} > 0.18$ and associated with area filling and chaotic orbits in the associated classical model, is plotted as a hatched blue histogram. Figure 6 illustrates that there is a difference between the quasi-energy distributions in the two subspaces. The distribution of quasi-energy spacings is closer to that of a random matrix theory in the ergodic subspace and closer to a Poisson model in the integrable subspace.

Figure 6a supports the Bohigas-Giannoni-Schmit (BGS) conjecture asserting that the spectral statistics of quantum systems whose classical counterparts exhibit chaotic behavior are described by random matrix theory[8]. Figure 6b suggests that the Bohigas-Giannoni-Schmit conjecture may in some cases apply to subspaces of a single quantum system with classical counterpart exhibiting regions of chaotic behavior.

IV. ESTIMATES FOR THE WIDTH OF THE CHAOTIC REGION

A. The width of the classical chaotic region at the separatrix

In a classical Hamiltonian system, a method akin to Melnikov's method for proving existence of chaotic behavior[36] can be used to estimate the size of the energy change caused by a perturbation near the separatrix orbit of the unperturbed system[15,48,57,64]. The width of the chaotic region formed at the separatrix connecting two hyperbolic fixed points is estimated by integrating the time dependent perturbation along the separatrix orbit that is present in the unperturbed system. The change in energy caused by the perturbation on the the separatrix orbit with momentum and angle $p_s(t), \phi_s(t)$ is

$$\Delta H = \int \frac{\partial H_1(\phi_s, p_s, t)}{\partial t} dt. \tag{48}$$

When applied to a perturbed pendulum, (equation 1) the energy change ΔH depends upon the Melnikov-Arnold integral[15,32,48]

$$A_m(\lambda) \equiv \int_{-\infty}^{\infty} \cos\left(\frac{1}{2} m \phi_s(t) - \lambda t\right) dt \tag{49}$$

on the separatrix trajectory

$$\phi_s(t) = 4 \arctan(e^t) - \pi. \tag{50}$$

For $\lambda < 0$, the result is typically small. For $\lambda > 0$ (and following[15,32])

$$A_1(\lambda) = 2\pi \frac{e^{\frac{\pi\lambda}{2}}}{\sinh(\pi\lambda)} \tag{51}$$

$$A_2(\lambda) = 2\lambda A_1(\lambda). \tag{52}$$

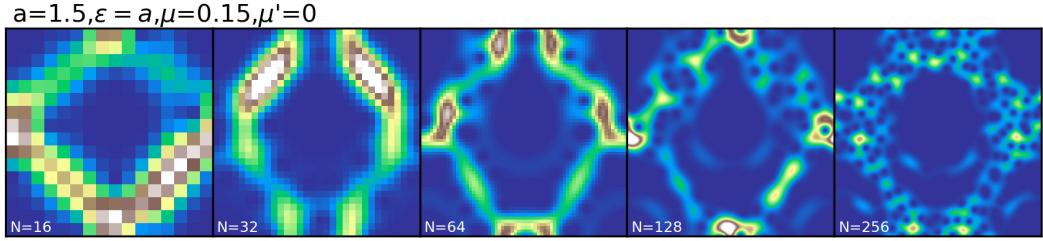$a=1.5, \varepsilon = a, \mu=0.15, \mu'=0$

FIG. 5. A sequence of Husimi distributions as a function of increasing dimension N. We show Husimi functions constructed from eigenstates of the Floquet propagator $\hat{U}_T$ that have energy near the separatrix for a Hamiltonian model with parameters printed on the top left side of the plot. Each panel shows a model that has the same parameters but has a different dimension N. The dimensions are printed on the bottom left of each panel and are powers of 2. This figure illustrates that in a region that is chaotic in the associated classical model, Husimi functions of the eigenstates appear increasingly diffuse and evenly distributed at larger N. This suggests that they belong to a subspace that is ergodic in the sense described by Shnirel'man[51].
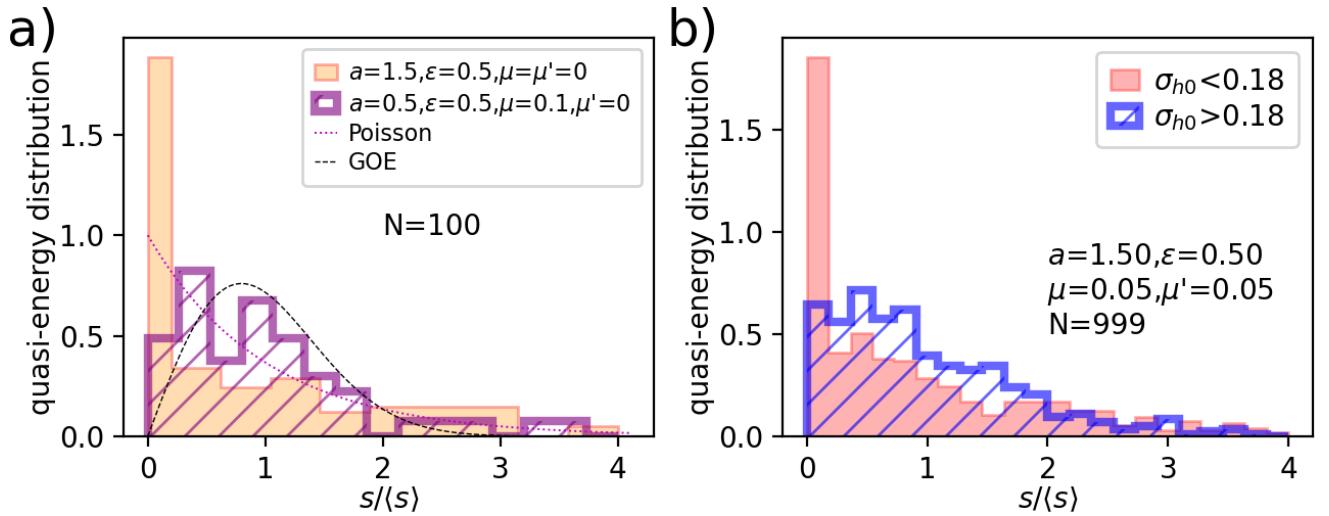

FIG. 6. Comparing distributions of quasi-energy spacings. a) On the left we compare the distributions of quasi-energy spacings for two quantum models. The solid orange histogram is derived from a classical integral model and is shown in Figure 1. The hatched purple histogram is derived from a classical model exhibiting chaotic regions and is shown in Figure 3. Histograms are normalized by the mean quasi-energy difference $\langle s \rangle$. The dotted magenta line shows a Poisson process with energy level differences $p(s) = e^{-s}$ with a mean of 1. The dashed black line shows the spacing distribution for the Gaussian orthogonal ensemble random matrix model (equation 47). b) We show quasi-energy spacings extracted from two subspaces in the system shown in Figure 2 but with $N = 999$ states. The solid pink distribution is constructed from the subspace of eigenstates with a high energy dispersion, $\sigma_{h0,j} > 0.18$, (as computed with equation 46) and the blue hatched histogram shows the distribution of the remaining eigenstates.

Following Shevchenko[48], for the particular pendulum system $H_0(p, \phi) = \frac{p^2}{2} - \omega_0^2 \cos\phi$ with perturbation $\mu \cos\phi \cos\tau$, the separatrix trajectory is that of equation 50 but with time rescaled by ω_0. The half width of the chaotic region near the separatrix is estimated as

$$\Delta H \sim \frac{\mu}{\omega_0} \left(A_2(\omega_0^{-1}) + A_2(-\omega_0^{-1}) \right)$$

$$\sim \frac{4\pi\mu}{\omega_0^2} \frac{e^{\frac{\pi}{2\omega_0}}}{\sinh(\pi/\omega_0)}. \tag{53}$$

The perturbation frequency is absent because we work with time in units of the perturbation frequency. Our factor $1/\omega_0$ represents the ratio of perturbation to pendulum libration frequency. Here we have neglected a relative phase shift for the

perturbation, but it is taken into account when generating separatrix maps[15,32,53,64]. Better approximations to the separatrix width take into account a series of strong resonances within the separatrix chaotic layer and are usually calculated in the weak perturbation limit of $\mu/\varepsilon \ll 1$[49,53].

Using an integral along the separatrix orbit, we similarly estimate the width of the chaotic region for special cases of the periodically perturbed Harper model of equation 6.

We estimate the width of the primary resonance using the energy of the separatrix orbit of the unperturbed system with energy ε, assuming $\varepsilon, a > 0$. The maximum momentum of this orbit satisfies $p_{\max} = 2\arcsin\sqrt{\varepsilon/a}$ which is narrow if $\sqrt{\varepsilon/a}$ is small. In the limit of small $\sqrt{\varepsilon/a}$, the primary resonance resembles a pendulum with $H_0(p, \phi) \sim ap^2/2 - \varepsilon\cos\phi$.

With perturbation $-\mu(\cos(\phi - \tau) + \cos(\phi + \tau))$, the energy change at the separatrix is that given by equation 53 but with $\omega_0 = \sqrt{\varepsilon/a}$.

In the case of $a = \varepsilon$, the energy of the two hyperbolic fixed points are the same and there is a single separatrix, otherwise there are two separatrices that separate phase space into 3 distinct regions, as seen in Figure 1a. The separatrix satisfies $\cos p = -\cos\phi$ or $p = \pm\phi + \pi$. Hamilton's equations give $\dot\phi = \partial_p H_0 = a\sin p$. On the separatrix orbit $\dot\phi = \pm a\sin\phi$ and $d\tau = \pm\frac{d\phi}{a\sin\phi}$. We integrate to find a separatrix orbit

$$\phi_s(\tau) = 2\arctan(e^{\pm a\tau}). \tag{54}$$

The sign specifies the particular segment of the separatrix. The trajectory resembles that of equation 50 for the pendulum's separatrix except for a factor of 2. The energy change for $\mu = \mu'$ depends upon the Melnikov-Arnold integral $A_1()$ instead of $A_2()$ giving half width energy estimate

$$\Delta H \sim \frac{2\pi\mu}{\omega_0}\frac{e^{\frac{\pi}{2\omega_0}}}{\sinh\pi/\omega_0}, \tag{55}$$

with $\omega_0 = a$ because $a = \varepsilon$ for this case. A comparison between equation 55 and equation 53 suggests that a general expression could be developed that interpolates between these cases. Though we found simple analytical forms for the separatrix orbits with $a \neq \varepsilon$ (equations 8 can be integrated to give expressions for $\phi_s(\tau)$), we have not found a simple analytical form for the integral along the separatrix in the more general case of the Harper model.

We computed the width of the chaotic region numerically from the energy dispersion for models with $a = \varepsilon$, $\omega_0 \sim 1$, and μ ranging from 0.01 to 0.1 and find that the chaotic region width estimated by equation 55 is a factor of a few lower than we measured. This is not inconsistent with more detailed and improved estimates for the chaotic zone width that are predominantly tested in the weak perturbation limit of $\mu/\varepsilon \ll 1$[49,53].

B. Averaging the Floquet propagator in the interaction representation

We derive an expression for ΔH, the width of the chaotic region and analogous to equation 48, but in the quantum regime. For some time dependent Hamiltonian systems, it can be efficient to compute a propagator using the interaction representation (or picture) as the Magnus expansion in this representation is more likely to converge (e.g.,[9,14,33]). In the interaction representation, with Hamiltonian operator $\hat{h} = \hat{h}_0 + \hat{h}_1(t)$, a sum of time independent and time dependent operators, state vectors are defined with a time-dependent unitary transformation

$$|\psi_I(t)\rangle = e^{i\hat{h}_0 t/\hbar}|\psi(0)\rangle. \tag{56}$$

The operator associated with perturbation operator $\hat{h}_1(t)$ is

$$\hat{h}_{1,I}(t) = e^{\frac{i}{\hbar}\hat{h}_0 t}\hat{h}_1(t)e^{-\frac{i}{\hbar}\hat{h}_0 t}. \tag{57}$$

For our quantum system with Hamiltonian in equation 15, with $\hbar = 2\pi/N$ (as discussed in section II A for our dimensionless Hamiltonian operator, see equation 25),

$$\hat{h}_{1,I}(\tau) = e^{\frac{iN}{2\pi}\hat{h}_0\tau}\hat{h}_1(\tau)e^{-\frac{iN}{2\pi}\hat{h}_0\tau} \tag{58}$$

$$= \sum_{j=0}^{\infty}\left(\frac{iN\tau}{2\pi}\right)^j\frac{1}{j!}[(\hat{h}_0)^j, \hat{h}_1(\tau)] \tag{59}$$

where in the second line we have used the Campbell identity[11] and short hand notation for repeated commutators (e.g., $[(\hat{h}_0)^3, \hat{h}_1] = [\hat{h}_0, [\hat{h}_0, [\hat{h}_0, \hat{h}_1]]]$ and $[(\hat{h}_0)^0, \hat{h}_1] = \hat{h}_1$).

In the interaction representation, the Floquet propagator of equation 25 becomes

$$\hat{U}_{T,I} = \mathscr{T}e^{\frac{Ni}{2\pi}\int_0^{2\pi}\hat{h}_{1,I}(\tau)d\tau}. \tag{60}$$

The Magnus expansion gives an time-independent effective or average Hamiltonian $h_{F,I}$, for a Floquet propagator such as in equation 60,[7,9,17,34]

$$e^{-iN\hat{h}_{F,I}} = U_{T,I}. \tag{61}$$

The expansion is the sum of a series of operators $\hat{\Omega}_n$

$$N\hat{h}_{F,I} = \sum_{n=1}^{\infty}\hat{\Omega}_n, \tag{62}$$

and the first two terms in the expansion are

$$\hat{\Omega}_1 = \frac{N}{2\pi}\int_0^{2\pi}\hat{h}_{1,I}(\tau)d\tau \tag{63}$$

$$\hat{\Omega}_2 = \left(\frac{N}{2\pi}\right)^2\frac{1}{2i}\int_0^{2\pi}d\tau_1\int_0^{\tau_1}d\tau_2[\hat{h}_{1,I}(\tau_1), \hat{h}_{1,I}(\tau_2)]. \tag{64}$$

The expansion must converge if

$$\frac{N}{2\pi}\int_0^{2\pi}\|\hat{h}_{1,I}(\tau)\|_2 d\tau < \pi \tag{65}$$

where $\|.\|_2$ denotes the matrix norm. In this section we adopt a perturbation operator (from equation 15) with $\mu = \mu'$

$$\hat{h}_1(\tau) = -\mu\cos\hat{\phi}\cos\tau \tag{66}$$

so that we can describe the strength of the time dependent perturbation with a single parameter, μ. With this perturbation

$$\frac{N}{2\pi}\int_0^{2\pi}\|\hat{h}_{1,I}(\tau)\|_2 d\tau \leq N|\mu|. \tag{67}$$

If the perturbation parameter μ is small enough, the Magnus expansion of the interaction propagator (equation 60) would definitively converge. We note that the convergence condition is not fulfilled in many practical applications of the Magnus expansion (e.g.,[7,28]).

The first operator, $\hat{\Omega}_1$ in the Magnus expansion propagator in the interaction representation, is first order in the perturbation parameter μ. Inspection of equation 64 and the interaction Hamiltonian of equation 59 implies the order of μ is

equal to the index of the operator in the expansion. The averaged Hamiltonian

$$\hat{h}_{F,I} \approx \frac{1}{2\pi} \int_0^{2\pi} d\tau \, \hat{h}_{1,I}(\tau) + \mathscr{O}(\mu^2). \tag{68}$$

Equation 68 shows that $\hat{h}_{F,I}$ is the average of the perturbation in the interaction representation and explains why we included a factor of N in the exponent on the lefthand side of equation 62 in our definition for $\hat{h}_{F,I}$. This equation suggests that the averaged Hamiltonian in the interaction representation could give a description for the separatrix width, similar to the integral of the perturbation along the separatrix in the classical setting which is also first order in perturbation parameter μ.

We compute $\hat{h}_{F,I}$ to first order in μ (using equation 59)

$$\hat{h}_{F,I} = \frac{1}{2\pi} \int_0^{2\pi} d\tau \sum_{j=0}^{\infty} \left(\frac{iN\tau}{2\pi}\right)^j \frac{1}{j!} [(\hat{h}_0)^j, \hat{h}_1(\tau)]. \tag{69}$$

The $j = 0$ term vanishes as as long as $\int_0^{2\pi} \hat{h}_1(\tau) = 0$, and this is obeyed by the perturbation in our model of equation 15. The $j = 1$ term vanishes because $\int_0^{2\pi} \tau \cos \tau d\tau = 0$. The first non-vanishing term is that with $j = 2$. For $j \geq 2$ we can integrate the integral $\int_0^{2\pi} \tau^j \cos \tau d\tau$ to find a general expression for the operator

$$\hat{h}_{F,I} = -\frac{\mu}{2\pi} \sum_{j=2}^{\infty} [(\hat{h}_0)^j, \cos \hat{\phi}] \left(\frac{iN}{2\pi}\right)^j$$
$$\times \left(\sum_{k=0}^{j} \frac{(2\pi)^{j-k}}{(j-k)!} \sin \frac{k\pi}{2} - \sin \frac{j\pi}{2}\right). \tag{70}$$

In appendix A we computed the commutators $[\cos \hat{p}, \cos \hat{\phi}]$ and $[\cos \hat{p}, \sin \hat{\phi}]$ (equations A12) and found that they were approximately proportional to $2\pi/N$. The factors of N would tend to cancel for each term indexed by j in equation 70. Probably the terms decrease in size, as the interaction Hamiltonian is bounded, but they might not decrease in size very quickly. We found that the eigenstates of $\hat{h}_0$ that are associated with stable fixed points in the associated classical model are approximately eigenstates of $\cos \hat{\phi}$ and so do not contribute to $\hat{h}_{F,I}$. The commutators in equation 70 determine which eigenstates (of $\hat{h}_0$) are most affected by the time dependent perturbation.

We denote an eigenstate of the unperturbed Hamiltonian $\hat{h}_0$ with energy E_j as $|v_j\rangle$ and use shorthand

$$E_{jk} = E_j - E_k. \tag{71}$$

We compute the matrix values for $\hat{h}_{F,I}$ using the eigenvectors of $\hat{h}_0$ in the interaction representation. The eigenstates of $\hat{h}_0$ in the interaction representation

$$|v_{j,I}(\tau)\rangle = e^{\frac{iN}{2\pi}E_j \tau} |v_j\rangle. \tag{72}$$

Matrix values for $\hat{h}_{F,I}$ (in the interaction picture) are

$$\langle v_{j,I}(\tau)| \hat{h}_{F,I} |v_{k,I}(\tau)\rangle = \frac{\mu i}{2\pi} (e^{iNE_{jk}} - 1) \frac{NE_{jk}}{2\pi} \frac{\langle v_j| \cos \hat{\phi} |v_k\rangle}{\left(\frac{NE_{jk}}{2\pi}\right)^2 - 1}$$
$$\times e^{-\frac{i}{2\pi}NE_{jk}\tau}. \tag{73}$$

Because we are working in the interaction picture, equation 61 implies that $\hat{h}_{F,I}$ is a perturbation to the Hamiltonian $\hat{h}_0$. In the Shrödinger picture, the Floquet propagator can be written in terms of a constant averaged Hamiltonian plus a perturbation $\mu \hat{V}$ evolved across a period of 2π,

$$\hat{U}_T = e^{-iN(\hat{h}_0 + \mu\hat{V})}. \tag{74}$$

Consequently, the matrix elements of the perturbation $\mu \hat{V}$ are equivalent to those computed in equation 73 via $\hat{h}_{F,I}$ at $\tau = 2\pi$,

$$V_{jk} = \langle v_j| \hat{V} |v_k\rangle = \frac{1}{\mu} \langle v_{j,I}(2\pi)| \hat{h}_{F,I} |v_{k,I}(2\pi)\rangle \tag{75}$$

$$= \frac{i}{2\pi} (e^{iNE_{jk}} - 1) \frac{NE_{jk}}{2\pi} \frac{\langle v_j| \cos \hat{\phi} |v_k\rangle}{\left(\frac{NE_{jk}}{2\pi}\right)^2 - 1} e^{-iNE_{jk}}. \tag{76}$$

To summarize, for the Hamiltonian in equation 15 but with $\mu = \mu'$ so that it has a single parameter describing the strength of the time dependent perturbation, we computed the first term in the Magnus expansion for the propagator $\hat{U}_T$ (defined equation 25) in the interaction picture. The result is given in equation 70 as an operator and with matrix elements in equation 73. This gave us an effective averaged perturbation in the Shrödinger representation with matrix elements that are given in equation 76.

C. Numerical estimates of the perturbation in the interaction picture

To test whether the matrix elements V_{jk} (of equation 76) match the behavior exhibited by the Floquet propagator of the periodically perturbed Harper model (equation 25), we display matrix elements of the Floquet propagator $\hat{U}_T$ along with matrix elements of $\hat{V}$ in Figure 7. Using the Trotter-Suzuki decomposition (described in section II B) we create the operator

$$\hat{U}(\tau) = \mathscr{T} e^{-\frac{iN}{2\pi} \int_0^\tau \hat{h}_{\text{PH}}(\tau') d\tau'} \tag{77}$$

integrated to times $\tau = \pi/2, \pi, 3\pi/2, 2\pi$. At the last time value, we have the full Floquet propagator $\hat{U}(2\pi) = \hat{U}_T$ (of equation 25). For each of these operators we compute the magnitude of the matrix elements $|\langle v_j| \hat{U}(\tau) |v_k\rangle|$ for $j, k \in [0, N-1]$. Here $|v_j\rangle$ are the eigenstates of the unperturbed Hamiltonian $\hat{h}_0$. Each pixel color in each panel shows the magnitude of a single matrix element, with pixels in order of the eigenstate energies. The times τ for each operator are shown in white on the lower left in each panel. The parameters for the periodically perturbed Harper Hamiltonian model (with Hamiltonian defined in equation 15) are printed on the top of the figure. For these models we set $\mu' = \mu$. We compute elements for the case $a = \varepsilon$ that has a single separatrix energy and a case with $a \neq \varepsilon$ which has two separatrices. The rightmost panels in Figures 7a and c show horizontal and vertical red lines at the separatrix energies. Figures 7a and c illustrate that the propagator has off-diagonal elements (in the

eigenbasis of the unperturbed Hamiltonian $\hat{h}_0$) near the separatrix energies. This is consistent and expected since ergodic regions in both quantum and associated classical system cover these separatrices.

In Figure 7b we similarly show the magnitudes of the matrix elements $|V_{jk}|$ computed via equation 76 for the same Hamiltonian parameters as in Figure 7a. Figure 7d is similar to Figure 7b except for the Hamiltonian parameters of Figure 7c. Figures 7b and d show that the perturbation operator $\hat{V}$ also has off-diagonal elements (in the $\hat{h}_0$ eigenbasis), near the separatrices. In this way the operator $\hat{V}$ is similar to the Floquet propagator. This implies that the approximations we have made in computing it (using only first operator in the Magnus expansion) have captured the key ability to cause perturbations at and near the separatrix energies.

Examining equations 70, 73, and 76, it is not obvious why the eigenstates of the unperturbed Hamiltonian $\hat{h}_0$ near the separatrix tend to give the largest off-diagonal matrix elements for $\hat{h}_{F,I}$ and $\hat{V}$. Strohmer and Wertz [55] approximated the energy spectrum of the unperturbed Hamiltonian $\hat{h}_0$ with a linear function (see Figure 1c), however our numerical computations show that the spacing between energy levels is reduced near the separatrices. This is expected as the phase space volume covered by a small range in energy dE is sensitive to the geometry of the Hamiltonian level curves and increases near the separatrix orbit. This is related to the relation between the derivative of the action with respect to energy and orbital period, with both quantities approaching infinity at the separatrix. As the volume in phase space sets energy level spacing via Bohr-Sommerfeld quantization, the increase in phase space volume within a particular dE, leads to a decrease in the energy spacing between eigenstates.

The factors that depend upon energy differences in equations 73 and 76 alone do not give larger magnitudes in V_{jk} for the eigenstates with energies similar to the separatrices. The matrix elements $\langle v_j | \cos \hat{\phi} | v_k \rangle$ (in equations 73 and 76) and the matrix elements of the commutators $[(\hat{h}_0)^n, \cos \hat{\phi}]$ (in equation 70) are banded in the sense that they decay rapidly away from the diagonal; (we found numerically that their magnitude rapidly drops as a function of increasing $|j-k|$). The banded behavior $\langle v_j | \cos \hat{\phi} | v_k \rangle$ means that the matrix elements of $\hat{V}$ given by equation 76 are largest near but not on the diagonal which vanishes due to the factor $e^{iNE_{jk}} - 1$. The denominator in equation 76, $\left(\frac{NE_{jk}}{2\pi}\right)^2 - 1$, is smallest for the terms near the separatrix where the difference between neighboring energy levels is smallest. Despite the simplicity of the Harper Hamiltonian when written in terms of clock and shift operators (see appendix A), we lack a simple analytical form for the separatrix eigenstates, making it difficult to see exactly why states near the separatrix energy tend to gives large values in equations 73 and 76.

D. Relating matrix elements of the perturbation to the energy dispersion

We relate the matrix elements in equation 76 of the perturbation $\hat{V}$ to the dispersion $\sigma_{h0,j}$ of the unperturbed Hamiltonian $\hat{h}_0$, that we numerically computed (in section III B) with the eigenstates of the propagator, $\hat{U}_T$. Equation 74 implies that the eigenstates of $\hat{U}_T$ are the same as the eigenstates of the operator

$$\hat{h}_0 + \mu \hat{V}. \tag{78}$$

In appendix B we show how to compute the dispersion of an unperturbed energy using the eigenstates of a non-degenerate and perturbed energy operator. The Harper Hamiltonian $\hat{h}_0$ can be written as a cyclic symmetric tridiagonal matrix with non-zero off-diagonal elements (see appendix A) and its eigenvalues probably distinct [55] (the operator is nearly tridiagonal and tridiagonal matrices with non-zero off-diagonal elements have distinct eigenvalues (Lemma 7.7.1 [38]). Equation 78 is in the form of equation B1, derived in appendix B. We apply equation B11 to estimate the dispersion $\sigma_{h0,j}$ (equation 46) of $\hat{h}_0$ but computed with the eigenstates of $\hat{h}_0 + \mu \hat{V}$ (which are also the eigenstates of $\hat{U}_T$)

$$\sigma_{h0,j}^2 = \mu^2 \sum_{j \neq k} |V_{jk}|^2. \tag{79}$$

We numerically compute $\sigma_{h0,j}/\mu$ using the matrix elements given in equation 76. The results are plotted as a function of j/N for 4 different unperturbed Hamiltonians in Figure 8. As we saw in Figure 7, peaks in Figure 8 also occur at the separatrices. These correspond to estimates for the standard deviation of the unperturbed energy operator computed from the eigenstates of the propagator, hence they are equivalent to those we computed from the numerically computed propagators and discussed in section III B. The peak values for $\sigma_{h0,j}/\mu$ we computed are fairly large, about 0.4. This size is large enough to be approximately consistent with the size of the standard deviations we measured directly from the eigenstates of the Floquet propagator in similar models (those shown in Figure 2c, and 3c).

Using equation 76

$$\sigma_{h0,j}^2 = \mu^2 \sum_{k \neq j} \left(\frac{NE_{jk}}{4\pi^2}\right)^2 \frac{|\langle v_j | \cos \hat{\phi} | v_k \rangle|^2}{\left(\left(\frac{NE_{jk}}{2\pi}\right)^2 - 1\right)^2} 2(1 - \cos(NE_{jk})). \tag{80}$$

As discussed at the end of section IV C, we found numerically that the sum is dominated by terms with k near but not equal to j because $|\langle v_j | \cos \hat{\phi} | v_k \rangle|$ decays away from its diagonal which vanishes due to the cosine factor. We suspect that the separatrix dominates because the spectrum of $\hat{h}_0$ has smaller energy level differences near the separatrix and this causes a small denominator in equation 80.

The adiabatic or low perturbation frequency limit is defined with the ratio of perturbation frequency to pendulum libration frequency $\lambda = \nu/\omega_0$, which for our dimensionless Harper
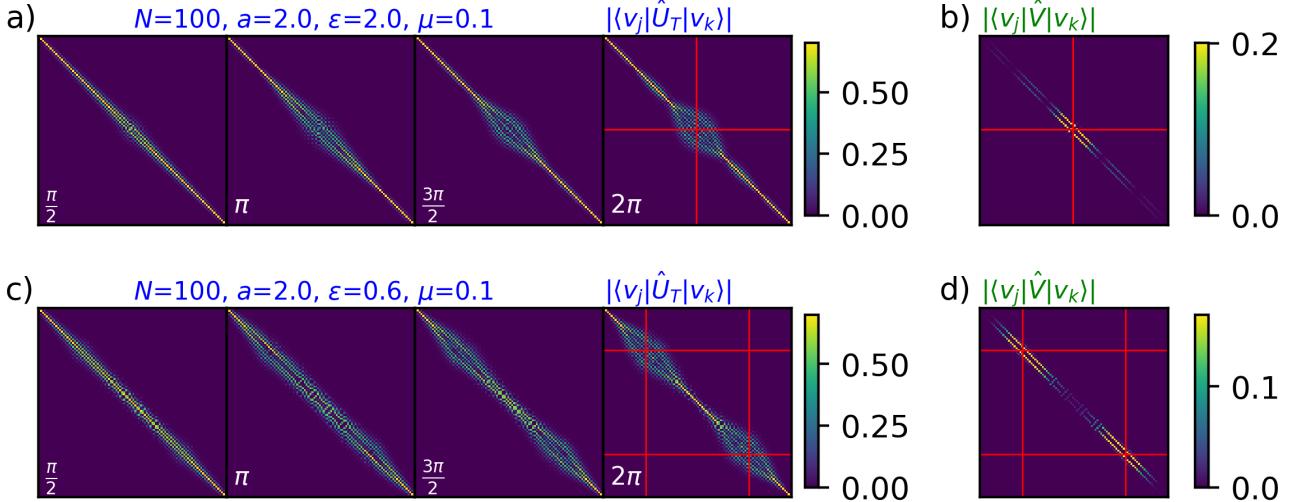
FIG. 7. a) The four panels on the left show the magnitudes of the matrix elements $|\langle v_j|\hat{U}(\tau)|v_k\rangle|$ (equation 77) constructed using eigenstates of unperturbed Hamiltonian $\hat{h}_0$. Each pixel shows different values of j,k and the eigenstates are in order of their energy. The 4 panels show $\hat{U}(\tau)$ integrated (via Trotterization) to 4 different times $\tau = 0, \pi/2, \pi, 2\pi$ with the Floquet propagator $\hat{U}_T$ (integrated to the full period of 2π) shown in the rightmost panel. In that same panel we show with red vertical and horizontal lines the locations of the eigenstates that have energies of the separatrices. The Floquet propagator $\hat{U}_T$ has strong off-diagonal elements near these separatrices. The parameters of the perturbed Harper Hamiltonian (equation 15) are printed on top in blue. For this model because $a = \varepsilon$, there is a single separatrix energy. b) For the same Hamiltonian shown in a) we show the magnitude of the matrix elements of $\hat{V}$ (equation 76), also constructed from eigenstates of $\hat{h}_0$. Again the off-diagonal elements are strongest near the separatrices which are shown with red horizontal and vertical lines. c) Similar to a) except for a Hamiltonian with different values of parameters a, ε. Because $a \neq \varepsilon$, there are two separatrix energies. d) Similar to b) except for the Hamiltonian of panel c). The Floquet propagator $\hat{U}_T$ and averaged perturbation operator $\hat{V}$ both contain off diagonal elements near the separatrices, indicating that $\hat{V}$ behaves similar to the Floquet propagator and can account for ergodicity generated near the classical separatrix orbits.

model is equal to ω_0^{-1} because we work with time in units of inverse perturbation frequency. In the non-adiabatic (or rapid perturbation) limit, classical estimates for the half width of the chaotic region decay exponentially (the ω_0 small limit in equation 53) with chaotic region width $\Delta H \propto e^{-\frac{\lambda\pi}{2}}$ [15]. If we adopt a characteristic energy $\tilde{\hbar}\omega_0 = \frac{2\pi}{N}\omega_0$ between states, then $\varepsilon_{jk} = \frac{NE_{jk}}{2\pi} \sim \omega_0(j-k)$. In the limit of small ω_0, equation 80 becomes $\Delta H \sim \varepsilon_{jk}^4 \sim \omega_0^4$. This decays rapidly as $\omega_0 \to 0$, consistent with the classically derived estimate, but with a steep power-law form rather than an exponentially decaying form. In the adiabatic limit, (ω_0 large), equation 80 gives $\Delta H \propto \varepsilon_{jk}^{-2} \propto \omega_0^{-2}$ and is similar to the classical expression, (though see [49,50,53,54] for improved calculations in the adiabatic limit).

Based on the estimates in this subsection and subsection IV B, we summarize how we estimated the energy width of the ergodic region for a Floquet quantum system. We consider a Hamiltonian $\hat{h}_0 + \hat{h}_1(t)$ with perturbation $\hat{h}_1(t)$ that is periodic with period T. We identify the energy E_s of a separatrix orbit in an associated classical system (that contains a hyperbolic fixed point) and an eigenstate $|v_s\rangle$ of the unperturbed system $\hat{h}_0$ that has energy close to E_s. We use the first term in the Magnus expansion within the interaction picture to compute an averaged perturbation (equations 57, 60, 61, 62, 63, and 68). Transfering back into the Shrödinger picture, we

estimate the width of the ergodic region near the separatrix using equation 79 and giving a width in energy

$$\Delta H \sim \sqrt{\sum_{k\neq s}\left|\langle v_s|\frac{1}{T}\int_0^T dt e^{\frac{i}{\hbar}\hat{h}_0 t}\hat{h}_1(t)e^{-\frac{i}{\hbar}\hat{h}_0 t}|v_k\rangle\right|^2} \quad (81)$$

where $|v_k\rangle$ are the eigenstates of $\hat{h}_0$. The sum is likely to be dominated by matrix elements for states $|v_k\rangle$ that have energy close to E_s, that of the separatrix.

Equation 81 for estimating the width (in energy) of a chaotic region at a separatrix is analogous to equation 48 in the classical setting (following [15,36,48,57,64]). Instead of using the separatrix orbit of the unperturbed classical Hamiltonian, equation 81 uses an eigenstate of the unperturbed system that is near the energy of the classical separatrix orbit. Instead of integrating the perturbation along the separatrix orbit, equation 81 sums over states with energies near that of the separatrix and the perturbation is averaged while undergoing evolution from the unperturbed system.

V. SUMMARY AND DISCUSSION

We have explored a doubly periodic in space (in angle and momentum) and periodic in time Hamiltonian dynamical system that can exhibit a hybrid or mixed phase space with both
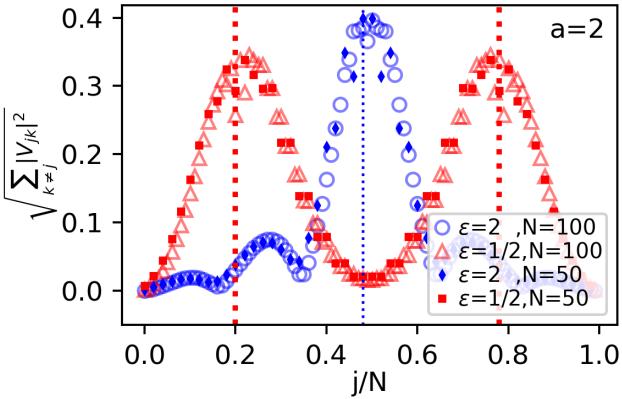
FIG. 8. We show estimates for the energy standard deviation $\sigma_{h0,j}/\mu$ for 4 different quantum systems (with Hamiltonian in the form of equation 15) and as a function of index j/N. The standard deviations are computed using equations 76 and 79 using the eigenstates of the unperturbed Hamiltonian $\hat{h}_0$. Parameters for the Hamiltonian are shown in the key and on the upper right. As in Figure 7, we compute the energy dispersion for models with two separatrices (open red triangles and small red squares) and models with a single separatrix (with $a = \varepsilon = 2$ and shown with open blue circles and filled small blue diamonds). The open points show models with number of states $N = 100$ and the filled points show models with $N = 50$. The energy standard deviation is not strongly dependent upon the number of states. States with energy near the separatrices are shown with vertical dotted lines. The energy standard deviations peak near states that have the energy of the separatrix in the associated classical model. The energy dispersion $\sigma_{h0,j}$ provides an estimate for the ergodicity of the eigenstates of the propagator $\hat{U}_T$ (as discussed in section III B) and can be estimated from the matrix elements of the perturbation in the interaction picture (as discussed in section IV B).

regular (non-ergodic) and chaotic (ergodic) motion in both classical and quantum settings. Our system is a periodically perturbed Harper model and is closely related to the periodically perturbed pendulum model discussed by Chirikov[15]. We chose to work with a compact phase space so that we can work in finite dimensional quantum spaces, facilitating numerical computation of the quantum Floquet progagator. We quantize the classical model by converting angle and momentum to a pair of operators that are related via discrete Fourier transform and using Bohr-Sommerfeld quantization to set the number of states from the area in phase space and Planck's constant. If the dimension of the system is odd, then this quantization method is equivalent to Wigner-Weyl quantization via the same point operator we use to make discrete versions of coherent states.

We used a discrete version of coherent states to compute Husimi functions showing phase space for the eigenstates of the Floquet propagator derived from the periodically perturbed Harper Hamiltonian. A comparison between Husimi functions and surfaces of section created for the associated classical system by directly integrating orbits shows remarkable similarity between morphology of orbits and eigenstates in phase space. We find that the expectation value for an eigenstate of the unperturbed energy operator and the mean

value for an orbit of the unperturbed energy function can be used to match eigenstates of the Floquet propagator to similar classical orbits. Moreover the energy dispersions computed for the Floquet eigenstates is similar to those computed from the classical orbits. The energy dispersion can be used to estimate which orbits and eigenstates are ergodic and gives an estimate for the width of a chaotic region that is generated near a separatrix of the unperturbed system.

Time dependent perturbation theory in quantum mechanics can fail to capture the behavior of a system because terms involved in the expansions are not small. We attempted Dyson series and Magnus expansions in the Shrödinger picture but they failed to give a model that captured the behavior near the separatrices seen in the periodically perturbed Harper model. The first term in the Dyson series is first order in the perturbation strength but the resulting computed operator is not unitary. Nonzero and complex high index terms in the Magnus expansion in the Shrödinger picture contain commutators that are first order in the perturbation strength. However, we found that the first term in the Magnus expansion in the interaction picture is first order in the perturbation strength and gives behavior similar to that seen in our system with large off-diagonal elements (in the eigenbasis of the unperturbed Hamiltonian) in the propagator at energy levels near that of the separatrices. Unfortunately, this Magnus expansion is only guaranteed to converge at a perturbation parameter below those used in our numerical exploration. A number of studies have found that the first few terms in a Magnus expansions are often useful even the full expansion does not converge (e.g.,[7,28]). Perhaps the averaged perturbation in the interaction picture is large in the same region where the propagator is large within the stationary phase approximation or the result is close to the correct one in a geometric sense. The stationary phase approximation has been effective for derivation, in the semi-classical limit, of the van Vleck propagator[58]. Alternatively a geometric approach (e.g., Törmä[56]) could help with improved perturbative methods for chaotic Floquet systems like the one we studied here. These and other approaches could be explored in future work on Floquet systems such as the perturbed Harper model.

An advantage of the Magnus expansion in the interaction representation is that the first term, which is an average of the perturbation operator in the interaction picture, is first order in the perturbation parameter. Because it is first order we used it to derive an estimate for the width in energy of ergodic region that is analogous to that derived in the classical setting by integrating the perturbation along the separatrix orbit. The width of the separatrix chaotic layer is only roughly approximated by the Melnikov-Arnold integral method (e.g., Soskin and Mannella[53]), so future studies could improve upon estimates in both classical and quantum settings.

The Hamiltonian of the Harper model is remarkably simple in terms of clock and shift operators (see appendix A). Its eigenstates can be approximated with Hermite polynomials[55]. Nevertheless, we had difficulty analytically calculating a quantum counterpart to the Melnikov-Arnold integral which gives an estimate for the width of the chaotic region. With more effort perhaps these analytical expressions could be used

to derive an simpler analytical estimate for the ergodic region width leveraging our approach (in section IV B and IV D). Other Hamiltonian systems, such as that studied by Yampolsky et al. [63], have simpler expressions for their eigenstates and for these it might be easier to derive analytical estimates for the width of an ergodic region, as did Yampolsky et al. [63].

The resonance overlap criterion[15] for the onset of classical chaos has recently been generalized to a quantum system[63]. The system of hard core particles in a box, studied by Yampolsky et al. [63] displayed contiguous patches of nearly unperturbed eigenstates, separated by strongly perturbed states. The periodically perturbed Harper model, studied here, exhibits similar phenomena, in that it also displays perturbed eigenstates, that have broad and diffuse ergodic Husimi distributions, separated by states that have narrow Husimi distributions that are similar to regular classical orbits. Yampolsky et al. [63] used matrix elements of the perturbation, computed using eigenstates of the unperturbed system (their equation 5) to estimate the width of the chaotic layer near resonance. Our expressions, such as equation 81 also includes an expectation of the perturbation at the separatrix to estimate the width of a chaotic region. In our study we did not focus on the resonance overlap criterion for the onset of chaos, rather we focused on the role of chaos induced at a separatrix, which was part of the derivation of the resonance overlap criterion[15]. Our study of the periodically perturbed Harper model is complimentary as we focused on discrete and time-periodic systems potentially more directly leading to applications in the realm of quantum computing and Floquet engineering.

The resonance overlap criterion and estimates for the Lyapunov time based on the periodically perturbed pendulum model have been widely applied to predict stability and timescales for evolution in celestial mechanics (e.g.,[21,35,39,40,60]). The strong connection between the behavior of the classical and quantum Harper model suggests that classical methods for predicting chaotic phenomena might be effectively applied to some quantum systems.

[1] Albash, T., Lidar, D.A., 2018. Adiabatic quantum computation. Reviews of Modern Physics 90, 015002. doi:doi:10.1103/RevModPhys.90.015002, `arXiv:1611.04471`.

[2] Appleby, D.M., 2005. Symmetric informationally complete-positive operator valued measures and the extended Clifford group. Journal of Mathematical Physics 46, 052107. doi:doi:10.1063/1.1896384, `arXiv:quant-ph/0412001`.

[3] Balazs, N.L., Voros, A., 1989. The quantized Baker's transformation. Annals of Physics 190, 1–31. doi:doi:10.1016/0003-4916(89)90259-5.

[4] Berry, M.V., 1989. Quantum Scars of Classical Closed Orbits in Phase Space. Proceedings of the Royal Society of London Series A 423, 219–231. doi:doi:10.1098/rspa.1989.0052.

[5] Berry, M.V., Tabor, M., 1977. Level Clustering in the Regular Spectrum. Proceedings of the Royal Society of London Series A 356, 375–394. doi:doi:10.1098/rspa.1977.0140.

[6] Björk, G., Klimov, A.B., Sánchez-Soto, L.L., 2008. Chapter 7, The discrete Wigner function. Progess in Optics 51, 469–516. doi:doi:10.1016/S0079-6638(07)51007-3.

[7] Blanes, S., Casas, F., Oteo, J., Ros, J., 2009. The Magnus expansion and some of its applications. Physics Reports 470, 151–238. URL: `https://www.sciencedirect.com/science/article/pii/S0370157308004092`, doi:doi:https://doi.org/10.1016/j.physrep.2008.11.001.

[8] Bohigas, O., Giannoni, M.J., Schmit, C., 1984. Characterization of Chaotic Quantum Spectra and Universality of Level Fluctuation Laws. Physical Review Letters 52, 1–4. doi:doi:10.1103/PhysRevLett.52.1.

[9] Brinkmann, A., 2016. Introduction to average Hamiltonian theory. I. Basics. Concepts in Magnetic Resonance Part A 45A, e21414. URL: `https://onlinelibrary.wiley.com/doi/abs/10.1002/cmr.a.21414`, doi:doi:https://doi.org/10.1002/cmr.a.21414.

[10] Bubner, N., Graham, R., 1991. Quantum dynamics in a chaotic separatrix layer. Phys. Rev. A 43, 1783–1790. doi:doi:10.1103/PhysRevA.43.1783.

[11] Campbell, J.E., 1897. On a law of combination of operators (second paper). Proceedings of the London Mathematical Society 28, 381–390.

[12] Cartwright, N.D., 1976. A non-negative Wigner-type distribution. Physica A Statistical Mechanics and its Applications 83, 210–212. doi:doi:10.1016/0378-4371(76)90145-X.

[13] Casati, G., Chirikov, B.V., Izraelev, F.M., Ford, J., 1979. Stochastic behavior of a quantum pendulum under a periodic perturbation, in: Casati, G., Ford, J. (Eds.), Stochastic Behavior in Classical and Quantum Hamiltonian Systems. volume 93, pp. 334–352. doi:doi:10.1007/BFb0021757.

[14] Chen, Y.H., Kalev, A., Hen, I., 2021. Quantum algorithm for time-dependent hamiltonian simulation by permutation expansion. PRX Quantum 2, 030342. URL: `https://link.aps.org/doi/10.1103/PRXQuantum.2.030342`, doi:doi:10.1103/PRXQuantum.2.030342.

[15] Chirikov, B.V., 1979. A universal instability of many-dimensional oscillator systems. Physics Reports 52, 263–379. doi:doi:10.1016/0370-1573(79)90023-1.

[16] Chirikov, B.V., Izrailev, F.M., Shepelyansky, D.L., 1988. Quantum chaos: Localization vs. ergodicity. Physica D Nonlinear Phenomena 33, 77–88. doi:doi:10.1016/S0167-2789(98)90011-2.

[17] Chu, S.I., 1985. Recent developments in semiclassical Floquet theories for intense-field multiphoton processes. Advances in Atomic and Molecular Physics 21, 197–253. URL: `https://www.sciencedirect.com/science/article/pii/S0065219908601438`, doi:doi:https://doi.org/10.1016/S0065-2199(08)60143-8.

[18] Farhi, E., Goldstone, J., Gutmann, S., Sipser, M., 2000. Quantum Computation by Adiabatic Evolution. arXiv e-prints , quant–ph/0001106doi:doi:10.48550/arXiv.quant-ph/0001106, `arXiv:quant-ph/0001106`.

[19] Fishman, S., Grempel, D.R., Prange, R.E., 1982. Chaos, Quantum Recurrences, and Anderson Localization. Physical Review Letters 49, 509–512. doi:doi:10.1103/PhysRevLett.49.509.

[20] Galetti, D., Marchiolli, M.A., 1996. Discrete Coherent States and Probability Distributions in Finite-Dimensional Spaces. Annals of Physics 249, 454–480. doi:doi:10.1006/aphy.1996.0079.

[21] Hadden, S., Lithwick, Y., 2018. A Criterion for the Onset of Chaos in

Systems of Two Eccentric Planets. Astronomical Journal 156, 95. doi:doi:10.3847/1538-3881/aad32c, arXiv:1803.08510.

[22] Harper, P.G., 1955. Single Band Motion of Conduction Electrons in a Uniform Magnetic Field. Proceedings of the Physical Society A 68, 874–878. doi:doi:10.1088/0370-1298/68/10/304.

[23] Hatano, N., Suzuki, M., 2005. Finding Exponential Product Formulas of Higher Orders, in: Das, A., Chakrabarti, B.K. (Eds.), Lecture Notes in Physics, Berlin Springer Verlag. volume 679, p. 37. doi:doi:10.1007/11526216_2.

[24] Heller, E.J., 1984. Bound-State Eigenfunctions of Classically Chaotic Hamiltonian Systems: Scars of Periodic Orbits. Physical Review Letters 53, 1515–1518. doi:doi:10.1103/PhysRevLett.53.1515.

[25] Iomin, A., Fishman, S., Zaslavsky, G.M., 2003. Semiclassical quantization of separatrix maps. Phys. Rev. E 67, 046210. doi:doi:10.1103/PhysRevE.67.046210.

[26] Izrailev, F.M., 1986. Limiting quasienergy statistics for simple quantum systems. Phys. Rev. Lett. 56, 541–544. URL: https://link.aps.org/doi/10.1103/PhysRevLett.56.541, doi:doi:10.1103/PhysRevLett.56.541.

[27] Kurlberg, P., Rudnick, Z., 2001. On quantum ergodicity for linear maps of the torus. Commun. Math. Phys. 222, 201–227.

[28] Kuwahara, T., Mori, T., Saito, K., 2016. Floquet-Magnus theory and generic transient dynamics in periodically driven many-body quantum systems. Annals of Physics 367, 96–124. doi:doi:10.1016/j.aop.2016.01.012, arXiv:1508.05797.

[29] Lebœuf, P., 1998. Normal and anomalous diffusion in a deterministic area-preserving map. Physica D Nonlinear Phenomena 116, 8–20. doi:doi:10.1016/S0167-2789(97)00250-9.

[30] Leonhardt, U., 1996. Discrete Wigner function and quantum-state tomography. Physics Review A 53, 2998–3013. doi:doi:10.1103/PhysRevA.53.2998.

[31] Lévi, B., Georgeot, B., 2004. Quantum computation of a complex system: The kicked Harper model. Physical Review Letters 70, 056218. doi:doi:10.1103/PhysRevE.70.056218, arXiv:quant-ph/0409028.

[32] Lichtenberg, A.J., Lieberman, M.A., 1992. Regular and Chaotic Dynamics. volume 38 of *Applied Mathematical Sciences*. 2nd ed., Springer-Verlag.

[33] Low, G.H., Wiebe, N., 2018. Hamiltonian Simulation in the Interaction Picture. arXiv e-prints , arXiv:1805.00675doi:doi:10.48550/arXiv.1805.00675, arXiv:1805.00675.

[34] Magnus, W., 1954. On the exponential solution of differential equations for a linear operator. Communications on Pure and Applied Mathematics 7, 649–673. URL: https://onlinelibrary.wiley.com/doi/abs/10.1002/cpa.3160070404, doi:doi:https://doi.org/10.1002/cpa.3160070404.

[35] Mardling, R.A., 2008. Resonance, Chaos and Stability: The Three-Body Problem in Astrophysics, in: Aarseth, S.J., Tout, C.A., Mardling, R.A. (Eds.), The Cambridge N-Body Lectures. Springer Dordrecht. volume 760 of *Lecture Notes in Physics*, pp. 59–96. doi:doi:10.1007/978-1-4020-8431-7_3.

[36] Mel'nikov, V.K., 1963. On the stability of a center for time-periodic perturbations. Trudy moskovskogo matematicheskogo obshchestva 12, 3–52.

[37] Neufeld, O., Podolsky, D., Cohen, O., 2019. Floquet group theory and its application to selection rules in harmonic generation. Nature Communications 10, 405. URL: https://doi.org/10.1038/s41467-018-07935-y, doi:doi:10.1038/s41467-018-07935-y.

[38] Parlett, B.N., 1998. The symmetric eigenvalue problem. SIAM's Classics in Applied Mathematics, Society for Industrial and Applied Mathematics.

[39] Petit, A.C., Pichierri, G., Davies, M.B., Johansen, A., 2020. The path to instability in compact multi-planetary systems. Astronomy & Astrophysics 641, A176. doi:doi:10.1051/0004-6361/202038764, arXiv:2006.14903.

[40] Quillen, A.C., 2011. Three-body resonance overlap in closely spaced multiple-planet systems. Monthly Notices of the Royal Astronomical Society 418, 1043–1054. URL: https://doi.org/10.1111/j.1365-2966.2011.19555.x, doi:doi:10.1111/j.1365-2966.2011.19555.x.

[41] Rivas, A.M.F., Ozorio de Almeida, A.M., 1999. The Weyl Representation on the Torus. Annals of Physics 276, 223–256. doi:doi:10.1006/aphy.1999.5942, arXiv:quant-ph/9904041.

[42] Rivas, A.M.F., Ozorio de Almeida, A.M., 2002. Hyperbolic scar patterns in phase space. Nonlinearity 15, 681–693. doi:doi:10.1088/0951-7715/15/3/309, arXiv:nlin/0104068.

[43] Rudner, M.S., Lindner, N.H., 2020. The Floquet Engineer's Handbook. arXiv e-prints , arXiv:2003.08252doi:doi:10.48550/arXiv.2003.08252, arXiv:2003.08252.

[44] Santhanam, M.S., Sheorey, V.B., Lakshminarayan, A., 1998. Chaos and exponentially localized eigenstates in smooth Hamiltonian systems. Physical Review E 57, 345–349. doi:doi:10.1103/PhysRevE.57.345, arXiv:chao-dyn/9704002.

[45] Saraceno, M., 1990. Classical structures in the quantized baker transformation. Annals of Physics 199, 37–60. doi:doi:10.1016/0003-4916(90)90367-W.

[46] Scharf, R., Sundaram, B., 1992. Quantum signatures of homoclinic tangles and separatrices. Phys. Rev. A 45, 3615–3628. doi:doi:10.1103/PhysRevA.45.3615.

[47] Schwinger, J., 1960. Unitary Operator Bases. Proceedings of the National Academy of Science 46, 570–579. doi:doi:10.1073/pnas.46.4.570.

[48] Shevchenko, I.I., 2000. Geometry of a Chaotic Layer. Soviet Journal of Experimental and Theoretical Physics 91, 615–625. doi:doi:10.1134/1.1320098.

[49] Shevchenko, I.I., 2008. The width of a chaotic layer. Physics Letters A 372, 808–816. doi:doi:10.1016/j.physleta.2007.08.028, arXiv:1312.7099.

[50] Shevchenko, I.I., 2012. Width of the chaotic layer: Maxima due to marginal resonances. Phys. Rev. E 85, 066202. doi:doi:10.1103/PhysRevE.85.066202, arXiv:1312.5564.

[51] Shnirel'man, A.I., 1974. Ergodic properties of eigenfunctions. Russian Math. Surveys 29.

[52] Simon, B., 1982. Almost periodic Schrödinger operators: A Review. Advances in Applied Mathematics 3, 463–490. URL: https://www.sciencedirect.com/science/article/pii/S0196885882800183, doi:doi:https://doi.org/10.1016/S0196-8858(82)80018-3.

[53] Soskin, S.M., Mannella, R., 2009. Maximal width of the separatrix chaotic layer. Phys. Rev. E 80, 066212. doi:doi:10.1103/PhysRevE.80.066212, arXiv:0908.0459.

[54] Soskin, S.M., Mannella, R., Yevtushenko, O.M., 2008. Matching of separatrix map and resonant dynamics, with application to global chaos onset between separatrices. Phys. Rev. E 77, 036221. doi:doi:10.1103/PhysRevE.77.036221.

[55] Strohmer, T., Wertz, T., 2021. Almost Eigenvalues and Eigenvectors of Almost Mathieu Operators. Springer International Publishing. volume 6 of *Applied and Numerical Harmonic Analysis*. pp. 77–96. URL: https://doi.org/10.1007/978-3-030-69637-5_5, doi:doi:10.1007/978-3-030-69637-5_5.

[56] Törmä, P., 2023. Essay: Where can quantum geometry lead us? Phys. Rev. Lett. 131, 240001. URL: https://link.aps.org/doi/10.1103/PhysRevLett.131.240001, doi:doi:10.1103/PhysRevLett.131.240001.

[57] Treschev, D., Zubelevich, O., 2010. The Separatrix Map. Springer Berlin Heidelberg, Berlin, Heidelberg. chapter 4. pp. 75–92. URL: https://doi.org/10.1007/978-3-642-03028-4_4, doi:doi:10.1007/978-3-642-03028-4_4.

[58] Vleck, J.H.V., 1928. The correspondence principle in the statistical interpretation of quantum mechanics. Proceedings of the National Academy of Sciences of the United States of America 14, 178–88. URL: https://api.semanticscholar.org/CorpusID:25375915.

[59] Wei, D., Arovas, D.P., 1991. Quasi-energy distributions in the kicked Harper model. Physics Letters A 158, 469–474. doi:doi:10.1016/0375-9601(91)90462-H.

[60] Wisdom, J., Peale, S.J., Mignard, F., 1984. The chaotic rotation of Hyperion. Icarus 58, 137–152. doi:doi:10.1016/0019-1035(84)90032-0.

[61] Wootters, W.K., 1987. A Wigner-function formulation of finite-state quantum mechanics. Annals of Physics 176, 1–21. doi:doi:10.1016/0003-4916(87)90176-X.

[62] Wootters, W.K., 2006. Quantum Measurements and Finite Geometry. Foundations of Physics 36, 112–126. doi:doi:10.1007/s10701-005-9008-x.

[63] Yampolsky, D., Harshman, N., Dunjko, V., Hwang, Z., Olshanii, M., 2022. Quantum Chirikov criterion: Two particles in a box as a toy model for a quantum gas. SciPost Physics 12, 035. doi:doi:10.21468/SciPostPhys.12.1.035, arXiv:2104.12193.

[64] Zaslavsky, G., Filonenko, N., 1968. Stochastic instability of trapped particles and the conditions of applicability of the quasilinear approximation. Zh. Eksp. Teor. Fiz 54, 1590–1602.

Appendix A: Harper Hamiltonian in terms of the clock and shift operators

We write the periodically perturbed Harper Hamiltonian (equation 15) in terms of the clock and shift operators $\hat{X}, \hat{Z}$, defined in equation 34. Using our momentum and angle operators $\hat{p}, \hat{\phi}$, as defined in equations 9 and 14, it is convenient to compute

$$\cos \hat{p} = \sum_{k=0}^{N-1} \cos \frac{2\pi k}{N} |k\rangle_F \langle k|_F$$
$$= \frac{1}{2} \sum_{k=0}^{N-1} (\omega^k + \omega^{-k}) |k\rangle_F \langle k|_F = \frac{1}{2}(\hat{X} + \hat{X}^\dagger) \quad \text{(A1)}$$

$$\cos \hat{\phi} = \frac{1}{2} \sum_{k=0}^{N-1} (\omega^j + \omega^{-j}) |j\rangle \langle j|f = \frac{1}{2}(\hat{Z} + \hat{Z}^\dagger). \quad \text{(A2)}$$

The unperturbed term of equation 15 can be written in terms of the clock and shift operators

$$\hat{h}_0 = a(1 - \cos \hat{p}) - \varepsilon \cos \hat{\phi}$$
$$= a - \frac{a}{2}(\hat{X} + \hat{X}^\dagger) - \frac{\varepsilon}{2}(\hat{Z} + \hat{Z}^\dagger). \quad \text{(A3)}$$

In the basis with $\hat{\phi}$ diagonal, $\hat{h}_0$ is a real, symmetric and periodic tridiagonal matrix

$$\hat{h}_0 = \begin{pmatrix} \alpha_0 & \beta & 0 & 0 & 0 & \ldots & \ldots & 0 & \beta \\ \beta & \alpha_1 & \beta & 0 & 0 & \ldots & \ldots & 0 & 0 \\ 0 & \beta & \alpha_2 & \beta & 0 & \ldots & \ldots & 0 & 0 \\ \vdots & & \ddots & & \vdots & & \ddots & & \vdots \\ 0 & 0 & \ldots & \beta & \alpha_j & \beta & \ldots & 0 & 0 \\ \vdots & & \ddots & & \vdots & & \ddots & & \vdots \\ 0 & 0 & 0 & \ldots & \ldots & \beta & \alpha_{N-3} & \beta & 0 \\ 0 & 0 & 0 & \ldots & \ldots & 0 & \beta & \alpha_{N-2} & \beta \\ \beta & 0 & 0 & \ldots & \ldots & 0 & 0 & \beta & \alpha_{N-1} \end{pmatrix} \quad \text{(A4)}$$

with off-diagonal elements $\beta = -a/2$ and diagonal elements $\alpha_j = a - \varepsilon \cos \frac{2\pi j}{N}$ with $j \in \{0, 1, ..., N-1\}$.

The perturbation terms

$$\hat{h}_1(\tau) = -\mu \cos(\hat{\phi} - \tau) - \mu' \cos(\hat{\phi} + \tau)$$
$$= -\frac{(\mu + \mu')}{2}(\hat{Z} + \hat{Z}^\dagger) \cos \tau$$
$$- \frac{(\mu - \mu')}{2i}(\hat{Z} - \hat{Z}^\dagger) \sin \tau. \quad \text{(A5)}$$

The Harper model has the nice property that it is simply written in terms of the shift and clock operators. In the form of equation A3 and in the $N \to \infty$ limit, (see Strohmer and Wertz [55]) $\hat{h}_0$ is equivalent to the operator known as the *almost Mathieu operator* [52].

The clock and shift operators obey the following relations

$$\hat{Z}\hat{X} = \omega \hat{X}\hat{Z} \quad \text{(A6)}$$
$$\hat{Z}^N = \hat{X}^N = \hat{I} \quad \text{(A7)}$$
$$\hat{Q}_{FT} \hat{X} \hat{Q}_{FT}^\dagger = \hat{Z} \quad \text{(A8)}$$
$$\hat{Q}_{FT}^\dagger \hat{X} \hat{Q}_{FT} = \hat{Z}^\dagger \quad \text{(A9)}$$

where $\hat{I}$ is the identity operator and $\omega = e^{2\pi i/N}$. These identities aid in computing various commutators.

Since our perturbation depends upon $\cos \hat{\phi}$, and our Hamiltonian contains $\cos \hat{p}$, we compute the commutators,

$$[\cos \hat{p}, \cos \hat{\phi}] = ((\cos \phi_N - 1) \cos \hat{\phi} - \sin \phi_N \sin \hat{\phi}) \cos \hat{p}$$
$$[\cos \hat{p}, \sin \hat{\phi}] = ((\cos \phi_N - 1) \sin \hat{\phi} + \sin \phi_N \cos \hat{\phi}) \cos \hat{p}, \quad \text{(A10)}$$

where

$$\phi_N = \frac{2\pi}{N}. \quad \text{(A11)}$$

In the limit of large N

$$[\cos \hat{p}, \cos \hat{\phi}] \sim -\frac{2\pi}{N} \sin \hat{\phi} \cos \hat{p}$$
$$[\cos \hat{p}, \sin \hat{\phi}] \sim \frac{2\pi}{N} \cos \hat{\phi} \cos \hat{p}. \quad \text{(A12)}$$

Appendix B: The energy dispersion computed from eigenstates of a perturbed system

Consider a Hermitian static (time independent) operator $\hat{h}_0$ that is perturbed with another static Hermitian operator $\hat{A}$

$$\hat{h} = \hat{h}_0 + \mu \hat{A} \quad \text{(B1)}$$

in a finite dimensional Hilbert space and with small real perturbation parameter μ. We take eigenstates of $\hat{h}_0$ with energy E_j to be $|v_j\rangle$ (here indexed by integer j) and those of $\hat{h}$ to be the set $|w_k\rangle$, here indexed by integer k. The indices span 0 to $N - 1$ where N is the dimension of the discrete quantum space. Conventional non-degenerate quantum perturbation theory gives an expression for the eigenstates of $\hat{h}$ as a series expansion in powers of μ. To second order in μ

$$|w_j\rangle = (1 + a_j) |v_j\rangle + \sum_{k \neq j} b_{jk} |v_k\rangle + \mathcal{O}(\mu^3) \quad \text{(B2)}$$

with

$$a_j = -\frac{\mu^2}{2} \sum_{k \neq j} \frac{|A_{kj}|^2}{E_{jk}^2} \quad \text{(B3)}$$

$$b_{jk} = \mu \frac{A_{kj}}{E_{jk}} + \mu^2 \sum_{l \neq j} \frac{A_{kl} A_{lj}}{E_{jk} E_{jl}} - \mu^2 \frac{A_{kj} A_{jj}}{E_{jk}^2}, \quad \text{(B4)}$$

using shorthand $A_{jk} = \langle v_j | \hat{A} | v_k \rangle$ and $E_{jk} = E_j - E_k$. To second order in μ

$$|b_{jk}|^2 = \mu^2 \frac{|A_{kj}|^2}{E_{jk}^2} \quad \text{(B5)}$$

$$a_j + a_j^* = -\mu^2 \sum_{k \neq j} \frac{|A_{kj}|^2}{E_{jk}^2}. \quad \text{(B6)}$$

We use these expressions to compute the expectation values of the unperturbed operator $\hat{h}_0$ using the eigenstates of $\hat{h}$,

$$\mu_{h0,j} = \langle w_j | \hat{h}_0 | w_j \rangle$$
$$= (1 + a_j + a_j^*)E_j + \sum_{k \neq j} |b_{jk}|^2 E_k$$
$$= E_j - \mu^2 \sum_{k \neq j} E_{jk} \frac{|A_{kj}|^2}{E_{jk}^2} \tag{B7}$$

$$\mu_{h0,j}^2 = E_j^2 - 2E_j \mu^2 \sum_{k \neq j} \frac{|A_{kj}|^2}{E_{jk}} \tag{B8}$$

$$\langle w_j | \hat{h}_0^2 | w_j \rangle = (1 + a_j + a_j^*)E_j^2 + \sum_{k \neq j} |b_{jk}|^2 E_k^2$$
$$= E_j^2 - \mu^2 \sum_{k \neq j} (E_j + E_k) \frac{|A_{kj}|^2}{E_{jk}}. \tag{B9}$$

Putting these together, the dispersion

$$\sigma_{h0,j}^2 = \langle w_j | \hat{h}_0^2 | w_j \rangle - (\langle w_j | \hat{h}_0 | w_j \rangle)^2$$
$$= \mu^2 \sum_{k \neq j} |A_{jk}|^2. \tag{B10}$$

Note that $\mu_{h0,j}$ (equation B7) is second order in μ but also depends on the inverse of the energy differences, whereas $\sigma_{h0,j}$ is first order in μ but only depends on the matrix elements.

To summarize, to second order in the perturbation parameter μ, and with no degeneracies, the energy dispersion (of the unperturbed Hamiltonian) computed with the eigenstates of the perturbed operator $\hat{h}$

$$\sigma_{h0,j} = \mu \sqrt{\sum_{j \neq k} |\langle v_j | \hat{A} | v_k \rangle|^2}. \tag{B11}$$

The term on the right is independent of the energy level differences and depends only the matrix elements of the perturbation $\hat{A}$ computed with the eigenstates of the unperturbed operator $\hat{h}_0$.